

CHARGE DISPERSION IN FISSION OF ^{233}U BY 20-85MeV PROTONS

Nuclear Charge Dispersion of Products in the Light-Mass Region
Formed in the Fission of ^{233}U by Protons of Energy 20-85 MeV

by

Heather Marshall

Department of Chemistry, McGill University

Submitted in partial fulfilment of the requirements for the degree
of Master of Science.

Abstract

The independent formation cross sections of ^{95}Nb and ^{97}Nb and the cumulative yields of ^{95}Zr , ^{97}Zr and ^{99}Mo from the fission of ^{233}U by protons were determined radiochemically for bombarding energies of 20, 30, 40, 50, 60, 72 and 85 MeV, and charge dispersion curves were constructed from these cross sections. The displacement of the most probable charge from stability was found to be between 2.9 and 3.2 charge units, and the full-width at half-maximum of the curves was about 2.9 charge units. These results are very close to those for the charge dispersion of the light-mass products of the fission of ^{235}U and ^{238}U in this energy range, and thus differ from those for the charge dispersion of the heavy mass products, which show a marked dependence on the neutron-to-proton ratio of the target. It is proposed that the extra neutrons in the heavier members of a set of isotopic fission targets appear in the heavy-mass fission fragments.

Nuclear Charge Dispersion
of Products in the Light-Mass Region
Formed in the Fission of ^{233}U
by Protons of Energy 20 - 85 MeV

by

Heather Marshall

A thesis submitted to the
Faculty of Graduate Studies and Research
in partial fulfilment of the requirements for the degree of
Master of Science

Department of Chemistry
McGill University
Montreal, Canada

September 1971

Table of Contents

List of Figures	iii
List of Tables	iv
Chapter 1	1
Introduction	1
The fission process	1
The liquid-drop model	1
Excited nuclei	2
Fission products	3
Review of previous work	7
Chapter 2	15
Experimental Procedures	15
Irradiations	15
Chemical processing	16
Separation of niobium	16
Separation of zirconium	17
Separation of molybdenum	17
Separation of copper	18
Measurement of activity and decay analysis	18
Calculation of cross sections	24
Errors	27
Chapter 3	28
Results	28
Chapter 4	46
Discussion	46
References	53

List of Figures

Figure 1.	Mass distributions for the fission of ^{238}U induced by protons of 10 - 150 MeV.	5
Figure 2.	The effect of isotopic charge dispersion of a variation of Z_p with mass.	8
Figure 3.	The effect on isotopic charge dispersion of a variation of N/Z_p with mass.	10
Figure 4.	$(Z_A - Z_D)$ as a function of bombarding energy, for various targets.	12
Figure 5.	The energies at which the excitation functions of heavy-mass fragments reach their maxima, and the FWHM of the charge dispersions, for various targets.	12
Figure 6.	The target holder.	14
Figure 7.	A peak in a γ -ray spectrum as recorded by a Ge(Li) detector and 1600-channel analyser.	22
Figure 8.	The annihilation radiation peak of ^{64}Cu .	22
Figure 9.	The excitation function of ^{95}Nb (independent yield).	31
Figure 10.	The excitation function of ^{97}Nb (independent yield).	31
Figure 11.	The excitation function of ^{95}Zr (cumulative yield).	32
Figure 12.	The excitation function of ^{97}Zr (cumulative yield).	33
Figure 13.	The excitation function of ^{99}Mo (cumulative yield).	34
Figures 14 - 19.	Charge dispersion curves at bombarding energies 30 - 85 MeV ($\ln \sigma$ vs N/Z).	36
Figure 20.	Charge dispersion curve at 85 MeV (σ vs N/Z).	42
Figure 21.	Charge dispersion parameters for the fission of ^{233}U , ^{235}U , and ^{238}U as a function of bombarding energy.	44
Figure 22.	Mass distributions from the thermal-neutron fission of ^{239}Pu and ^{241}Pu .	51
Figure 23.	Mass distributions from the thermal-neutron fission of ^{233}U and ^{235}U .	51

List of Tables

Table I	Energies and abundances of γ -rays observed.	20
Table II	Cross sections for the monitor reaction $^{65}\text{Cu}(p, pn)^{64}\text{Cu}$.	24
Table III	Formation cross sections.	29
Table IV	Parameters of charge dispersion curves for ^{233}U .	43
Table V	Parameters for charge dispersion curves for ^{233}U , ^{235}U , and ^{238}U .	45
Table VI	Neutron emission characteristics of the compound nucleus and the heavy fragment for the proton-induced fission of ^{233}U , ^{235}U , and ^{238}U .	47
Table VII	Comparison of ^{233}U and ^{235}U fission.	50
Table VIII	Comparison of ^{233}U and ^{238}U fission.	50

Chapter 1

Introduction

The Fission Process

Although it is possible to describe many nuclear reactions in detail, and to predict results from empirical formulae, there is as yet no definitive model of the nucleus and no comprehensive theory of nuclear behaviour. Current nuclear technology rests on a great body of empirical knowledge while scientific investigations continue to clarify that knowledge and to illuminate the processes involved.

The liquid-drop model

The earliest formulation of a model of the nucleus was that of Bohr and Wheeler (1939). The nucleus is assumed to have liquid properties such as incompressibility and surface tension and so to behave in many ways as a liquid drop. The nucleus has additional properties due to the presence of charged as well as neutral particles in its composition. A nucleus in the ground state is spherical as a result of the surface tension. (It should be noted that all nuclei are not spherical, a fact which cannot be explained by the liquid-drop model alone.) An excited nucleus vibrates through various deviations from sphericity. If during the course of these vibrations the nucleus attains a deformation such that the decrease in the energy of coulombic repulsion among the protons is greater than the increase in the surface energy, it will not be restored to its equilibrium spherical state but will continue to distort and split into two individual deformed drops which are then driven apart by their mutual coulombic repulsion. Bohr and Wheeler showed that ground-state nuclei are unstable to these deformations if the parameter Z^2/A is greater than 44.8. The quantity $x = \frac{Z^2/A}{Z^2/A \text{ critical}}$ is known as the

fissionability parameter. Species with a fissionability parameter which is near one do not fission spontaneously, but are susceptible to induced fission at low excitation energies. Heavy nuclei, by virtue of their size, can also exist in extremely long deformed states, effectively lowering the coulomb barrier to fission by allowing the two major segments of the nucleus to be relatively far apart.

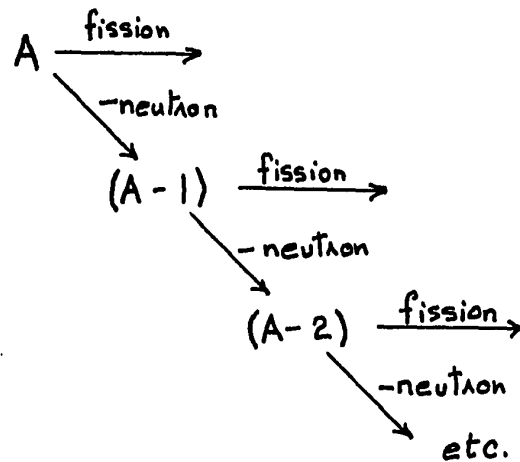
Excited nuclei

An excited nucleus can de-excite by the emission of γ -rays. If the excitation energy is greater than the energy binding neutrons into the nucleus, a neutron can be emitted, de-exciting the nucleus by the binding energy of that neutron plus its kinetic energy after emission. Protons or more complex charged particles may be emitted by a nucleus having enough excitation energy to overcome the coulomb barrier as well as contributing the binding energy. (An unstable species in its ground state cannot emit neutrons or protons, but some emit α particles, since the nucleons may be more tightly bound in the α particle than in the original nucleus, and so the system is more stable after α emission.) An excited fissionable nucleus can de-excite by fissioning as well as by nucleon emission.

Heavy nuclei may be excited and induced to fission by bombardment with neutrons, protons, or heavier particles. At low bombardment energies the projectile is absorbed into the nucleus, and the added energy distributed through the whole compound nucleus. At energies in the order of 50 MeV the mechanism becomes that of direct interaction between the projectile and a few of the nucleons within the nucleus. The incoming particle strikes one nucleon, giving it some kinetic energy and momentum. These two nucleons then continue to travel through the nucleus, striking other particles in their paths. The original projectile or any of the later members of the

cascade may reach the surface of the nucleus with enough kinetic energy to overcome the binding energy and escape. Thus the excited nucleus remaining after an intranuclear cascade has neither the mass of the original system, nor all the excitation energy which could have been delivered by the projectile.

Once a heavy nucleus is excited, there is a competition among the means of de-excitation. At the excitation energies encountered in the present work, it may be assumed that there is no charged particle emission, thus the major means of de-excitation are neutron emission and fission. In general at least one or two neutrons are emitted before the residual nucleus fissions, though the number of neutrons emitted is variable within a collection of identical nuclides, and there can be an array of fissioning nuclei.

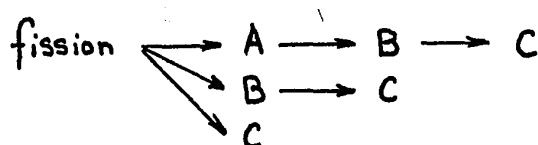


It should be noted that the ratio of the probability of neutron emission to that of fission decreases rapidly along this chain. At the point of fission several neutrons may be released or small fragments formed as the two major fragments separate.

Fission products

The fragments resulting from the fission of an excited nucleus retain between them the original excitation energy both as excitation and as

kinetic energy. Since the ratio of neutrons to protons in a stable species increases with increasing atomic number, the fission fragments are likely to be neutron-excessive in the energy region studied. Thus the fragments readily emit several neutrons immediately after fission as a means of de-excitation. The fission products which are usually observed in radiochemical studies are these fragments after they have emitted several neutrons and also given up their kinetic energy and come to rest. Many of these products are unstable to β -decay and have very short half-lives. Thus in many cases the yield of an observed product is the sum of its fission yield and the fission yields of its short-lived precursors. In these cases the result must be recognized as a



cumulative yield for the decay chain, and not the actual independent yield of the single observed species.

The independent yields of members of a β -decay chain may be determined radiochemically by a series of timed extractions; that is, by chemically separating a product from its precursors and the target material at several different times and then solving the set of equations giving the activities of these various samples as functions of time. The electron cloud surrounding a nucleus is violently disrupted by the fission of that nucleus. X-rays emitted as the electrons arrange themselves in the shells around the resulting fragments are characteristic of the various fragment species, and the study of these X-ray cascades offers a means of determining independent yields. Physical methods such as mass separation of the fission products, and time-

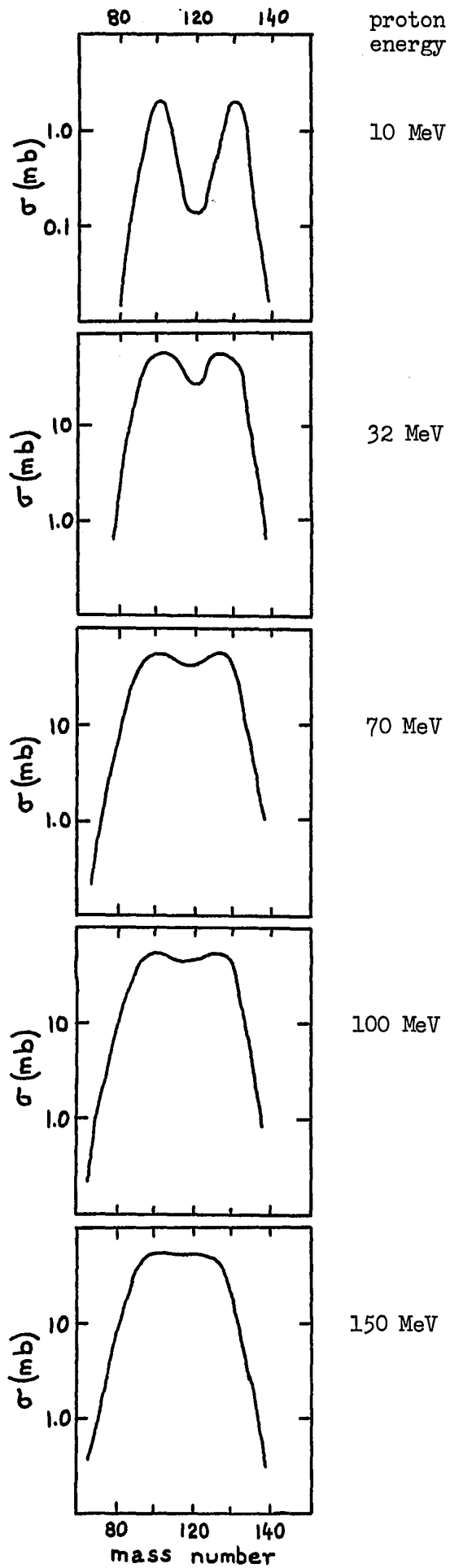


Figure 1.
Mass distributions for the fission of ^{238}U induced by protons of energies of 10 - 150 MeV.
(After Stevenson et al, 1958)

of-flight determinations of the energies and masses are also of great use. In some cases a stable or very long-lived species A_Z shields the species ${}^A_{(Z+1)}$ from production of β -decay. Clearly the independent yields of shielded nuclides are easily determined, but the presence of stable or long-lived species makes it difficult to determine the total yield for a given product mass. Knowledge of the charge dispersion function at any mass would make these determinations possible by means of simple integration.

The mass distribution of the products of fission has been studied extensively for most fissionable species. In general, at low excitation energies the distribution shows two peaks separated by a deep valley; the nucleus tends to fission asymmetrically. At higher excitation energies the valley fills up as symmetric fission becomes more probable, eventually giving a single smooth peak (Figure 1). At very low excitation energies (as imparted by thermal neutrons) fine structure is observed in the peaks. This fine structure is thought to be due to shell effects; for instance, a sharp spike at $A=134$ may be attributed to the stability imparted by the double shell closure at $Z=50$ and $N=82$.

It is possible to predict the yields of fission products from existing empirical results, but the laws governing the division of mass and charge between fission fragments are not known. It is the aim of the present work to contribute to knowledge concerning the division of charge in the fission process, specifically at proton bombardment energies in the range 20-85 MeV.

Review of Previous Work

In 1951 Glendenin et al reviewed the existing theoretical postulates describing charge distribution in the light of studies of the fission products of ^{235}U and ^{239}Pu and proposed the empirical formula of equal charge displacement (ECD). The available data indicated that the most likely charges of complementary products of thermal-neutron fission were equally removed from the most stable charges for their respective masses. The postulate of unchanged charge distribution or constant charge ratio (UCD or CCR) of Sugarman and of Goeckermann and Perlman (1949) leads to fission fragments having the same ratio of charge to mass as the fissioning nucleus. Product distributions derived under this postulate by estimating the number of neutrons emitted before and after fission were not consistent with the data. The postulate of Way and Wigner (1951) that the fission split occurs in such a way that the nuclear potential energy plus the coulombic energy of the fragments, just at scission, be at a minimum did not predict the experimental results. A similar and also unsuccessful proposal by Present (1947) included the asymmetry of charge distribution between unequal fragments (assumed to be spherical) due to the radial non-uniformity of charge density within each sphere. Since, in the formalism of the liquid drop model, charge drifts to the surface, then the smaller fragment would have a greater ratio of charge to mass.

Folger et al (1955) proposed that if the independent yields of members of a decay chain were assumed to be distributed about the most probable charge in a manner approximated by a Gaussian curve, then three points could define the charge dispersion curve. This non-theoretical choice of the form of charge dispersion curves was followed by others, including Wahl et al (1962), Pate et al (1958), Forster et al (1966), and Hogan and Sugarman (1969).

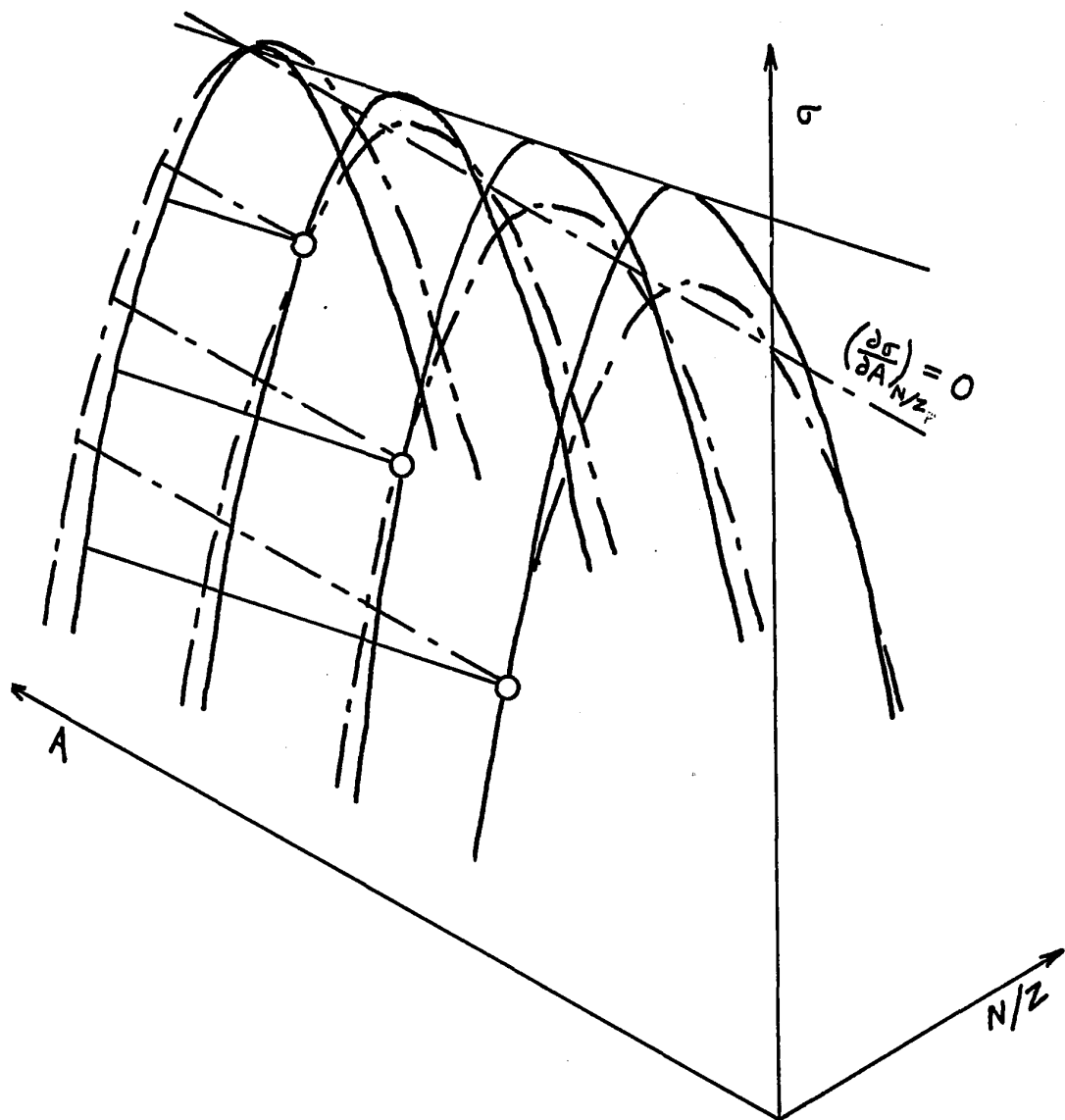


Figure 2. The effect of isotopic charge dispersion of a variation of σ with mass. The dashed line is a line satisfying the condition $(\frac{\partial \sigma}{\partial A})_{N/Z} = 0$. The dashed curves are the charge dispersion derived from the three experimental cross sections under the assumption of a flat mass-yield curve. If this assumption is false, the dashed curves are incorrect. The solid curves are the true dispersions related to the mass dependence indicated by the solid line. While N/Z_p is not affected by the false assumption, the shape and width of the dispersion are.

As the body of data grew for various target species induced to fission by various means, it became apparent that the ECD rule did not predict the results consistently (Colby and Cobble, 1961) and that the UCD postulate was more successful than had been indicated by Glendenin et al, though it was by no means definitive. At the same time, the minimum potential energy models were revised by Swiatecki and Blann (1960). Their predictions were shown to agree with data from low-energy fission (Coryell et al, 1961). As expected, the charge dispersion curves seemed to be distorted by the effects of shell edges (Wahl, 1958; Colby and Cobble, 1961).

Most of the early studies in charge dispersion were carried out by converting experimental independent yields to fractional chain yields (i.e. giving the yield of a species in terms of its contribution to the total yield for the isobaric chain of which it is a member) and drawing plots of fractional chain yield as a function of distance from stability (i.e. the number of β -decays the species must undergo to become a stable species). Inherent in this approach is the assumption that the charge dispersion function is independent of mass with respect to both the shape of the curve and the position of the peak (expressed as $Z_A - Z_p$, where Z_A is the most stable charge at mass A and Z_p the most probable). A further assumption is that the total chain yields can easily be determined. Friedlander et al (1963), in studying the fission of uranium with high-energy protons, proposed that the abscissa be drawn in terms of N/Z (neutron-to-proton ratio) rather than $(Z-Z_A)$, thus avoiding the discontinuity of Z_A at the neutron shell edges. They also assumed the mass-yield curve to be flat in the narrow mass region of the products studied. The actual independent yields could then be plotted directly to give isotopic charge dispersion curves. If the assumption is

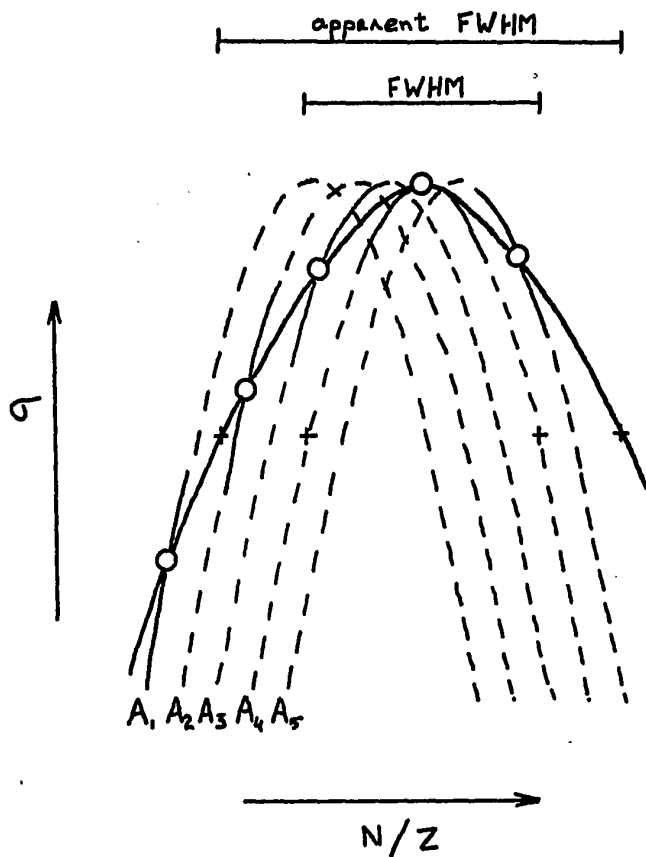


Figure 3. The effect of isotopic charge dispersion of a variation of N/Z_p with mass. The dashed curves are the actual charge dispersions, assumed to be the same shape at the different mass numbers. If there is no variation of N/Z_p with mass, the five curves may be superimposed to give a clear picture of their shape. If each curve is displaced along the N/Z axis, the curve drawn through the experimental cross sections will be broader than the true charge dispersion.

false, the curves are distorted by this approach, but the value of N/Z_p is not affected, as shown in Figure 2. The distribution curves found by Friedlander et al do not appear to be Gaussian at the lower energies studied, and not only broaden with increasing energy, but actually show a marked valley at energies higher than 0.68 GeV. There were sufficient data at each energy for the curves to be drawn by hand rather than be restricted to a simple function. Friedlander et al showed that the restraint placed by the experimental cumulative yields on those obtained by the addition of the independent yields taken from the curves for the same chains was sufficient to define the charge dispersion curves in regions where independent yields were not available. The mass of the nuclide nearest the peak of each curve was used to define Z_p from the empirical N/Z_p and to determine Z_A , thus giving $(Z_A - Z_p)$.

In plotting independent yields directly to give isobaric charge dispersion curves, it is assumed that N/Z_p is independent of mass over the range of the products studied. Hogan and Sugarman (1969) constructed a curve giving N/Z_p as a function of mass. Thus charge dispersion curves can be plotted with a scale of $(N/Z - N/Z_p)$ on the abscissa, where N/Z_p need not be assumed constant, but is known. Clearly this correction will not affect the value of N/Z at the peak of the distribution, but will alter the apparent width (Figure 3).

Forster et al (1966) noted a dependence of Z_p and of $\bar{\nu}_T$ (the average number of neutrons emitted per fission) on the target species. Tomita and Yaffe (1969) combined the existing charge dispersion results from the fission with medium energy protons of ^{238}U (Davies and Yaffe, 1963) and of ^{232}Th (Benjamin et al, 1969) with results from the fission of ^{233}U to outline a relation between $(Z_A - Z_p)$ and the neutron-to-proton ratio of the target nucleus.

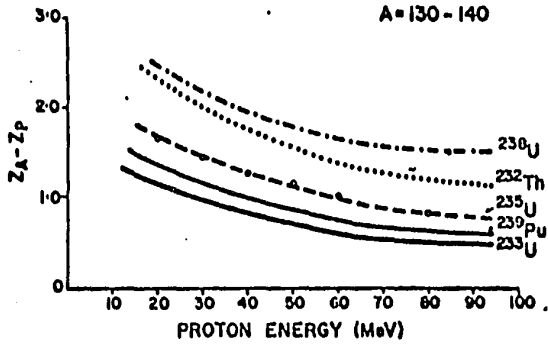


Figure 4.
Displacement of the most probable charge from stability for various targets.
(From Yaffe, 1969)

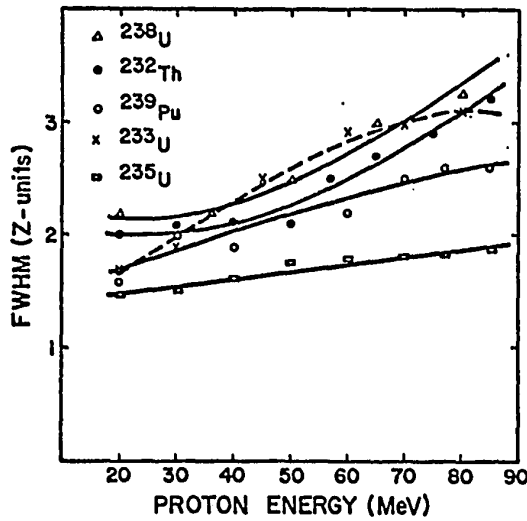
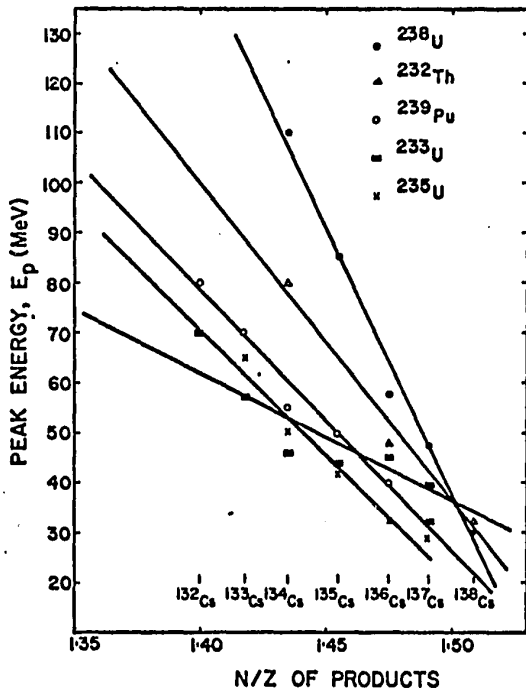


Figure 5. The energies at which the excitation functions of heavy-mass fragments reach their maxima, and the full-width at half-maximum of the charge dispersions, for various targets.
(From Saha et al, 1971)

Their predictions concerning the fission products of ^{239}Pu and ^{235}U were borne out by the work of Saha and Yaffe (1970) and Saha et al (1971). The results are shown in Figure 4, taken from Yaffe (1969). Tomita and Yaffe and later Saha and Yaffe noted a target dependence of the peaking energies of the fission product excitation functions and of the widths of the charge dispersions. Figure 5, taken from Saha et al, illustrates these.

The results discussed by Yaffe (1969) are derived from data for the mass range $A = 129 - 139$, i.e. for the heavy products of asymmetric fission. Khan et al (1970) investigated light products ($A = 90 - 93$) of the fission of ^{235}U and ^{238}U and found no target dependence in the behaviour of $(Z_A - Z_p)$ or the widths of the charge dispersions. The aim of the present work is to study the charge dispersion in the light mass region of the fission of ^{233}U and thus supplement the results of Khan et al.

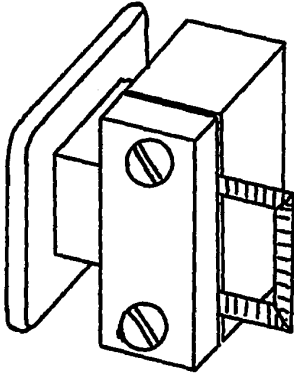


Figure 6. The target holder with a target clamped in place.

circulating beam of the McGill synchrocyclotron located at the Foster Radiation Laboratory. The beam current was of the order of 0.5 - 1 A and the duration of the irradiations was 10 - 20 minutes. The energy spread of the beam was taken to be ± 2 MeV.

Chemical Processing

After bombardment the target was dissolved in concentrated hydrochloric acid and concentrated nitric acid. 20 mg inactive niobium, 20 mg zirconium, 10 mg molybdenum, 10 mg strontium, and 5 mg tellurium were added, while the copper monitor acted as its own carrier.

Separation of niobium

Niobic acid was precipitated by adding $KClO_3$ and heating to oxidize the niobium. The precipitate was washed twice with $6N$ HNO_3 and dissolved in conc HCl. The solution was diluted to be $\sim 3N$ in HCl and twice treated by the addition of 10 mg Te(IV) and the reduction of this carrier to its metallic state with $NaHSO_3$. After the removal of the bulk of this precipitate the solution was scavenged with AgCl to remove any finely divided tellurium which remained. Niobic acid was reprecipitated by neutralizing the solution with conc NH_4OH and then dissolved in 20 drops HF. 1 ml $6N$ HNO_3 and 5 ml water were added and any contaminant zirconium removed by the addition of 10 mg Zr carrier and its precipitation as $ZrBaF_6$. The niobic acid was again recovered by neutralization of the solution, after the addition of 10 ml 5% HBO_3 to complex the fluoride ion which would otherwise complex the niobium and keep it in solution. The precipitate was washed with 2% NH_4NO_3 and then with hot conc HNO_3 , heated at $800^\circ C$ for 15 minutes, and weighed as Nb_2O_5 .

Separation of zirconium (Flynn et al, 1960)

The target solution was extracted with 15 ml 0.4M TTA (thenoyltrifluoroacetone) in benzene for 10 minutes, and the benzene layer washed three times with 10 ml portions of 1N HNO₃. The zirconium was back-extracted into 10 ml 2N HF and BaZrF₆ precipitated by the addition of 50 mg Ba²⁺, washed with 10 ml water, and dissolved in 3 ml 5% H₃BO₃. After the addition of 1 ml conc HNO₃ and 5 ml water, the barium was removed as BaSO₄ by the addition of 0.5 ml H₂SO₄. The zirconium was precipitated as the hydroxide with NH₄OH and then redissolved in 2 ml HCl. This solution was diluted with 8 ml water, 10 ml 16% mandelic acid were added and the solution heated on steam for 10 minutes to precipitate Zr(C₆H₅CHOHCOO)₄. The precipitate was washed with water, alcohol, and ether and dried at 110°C for 10 minutes.

Separation of molybdenum (Wiles and Coryell, 1954)

The nitric acid in the target solution was destroyed by boiling with 10-12 ml HCl. 2 mg Fe³⁺ carrier were added and the molybdenum and iron extracted into 100 ml diethyl ether which had been equilibrated with 6N HCl. The ether layer was washed twice with 2 ml portions of 6N HCl and then back-extracted with two 10 ml portions of water. Fe(OH)₃ was precipitated with NH₄OH and the solution scavenged again with 1 mg additional iron. (Fission products which may be co-extracted and then removed with the Fe(OH)₃ are Ga, Tc, As, Ge, Te, Sn, Sb, I and Br.) 10 mg rhenium carrier were added, the solution made just acidic to methyl orange with HCl, then buffered with 5 ml 5% NaC₂H₃O₂ and brought nearly to boiling. The molybdenum was precipitated with 1 ml 5% 8-hydroxyquinoline in 1N HCl. The precipitate MoO₂(C₉H₆ON)₂ was washed with water, alcohol, and ether and dried at 110°C for 15 minutes.

Separation of copper

After the removal of the desired fission products the target solution was made basic with NH_4OH and then just acidic with HCl . The copper monitor was precipitated as CuS with a few drops of ammonium sulfide. The CuS was dissolved in ~ 1 ml conc HCl and the solution adsorbed on a column of Dowex 1-X8 200-400 mesh anion exchange resin prepared with 10N HCl . The column was washed with 4N HCl to remove zinc, cobalt, and iron, and the copper eluted with 2.5 N HCl . The solution was diluted to be $\sim 1\text{N}$ in HCl , the copper reduced with NaHSO_3 , and CuCNS precipitated by the dropwise addition of 2.5M NH_4SCN . The precipitate was washed with ethanol and dried at 110°C . The method is based on the work of Kraus and Moore (1953), and has been used in this laboratory for several years.

In each case the final precipitate was collected on a glass fibre disc clamped between a filter chimney and a Millipore filter. The disc was fixed on the centre of a piece of cardboard and covered with Mylar, making a counting sample of reproducible geometry.

Measurement of Activity and Decay Analysis

The probability of decay of an excited nucleus is constant with respect to time. Thus for a collection of excited nuclei, the number decaying at a given time must be proportional to the number present.

$$-\frac{dN}{dt} = \lambda N$$

where N is the number of nuclei

λ is the decay constant

t is time

giving
$$N = N^0 e^{-\lambda t} \quad (1)$$

where N^0 is the value of N when

$$t = 0$$

and
$$D = \lambda N = \lambda N^0 e^{-\lambda t}$$

where D is the disintegration rate.

The disintegration rate of a species in the presence of its active parent is not necessarily a monotonically decreasing function of time, since the daughter is being produced as well as decaying. Denoting the parent by A and the daughter by B,

$$\begin{aligned}\frac{d N_B}{d t} &= \text{production of B} - \text{decay of B} \\ &= \text{decay of A} - \text{decay of B}\end{aligned}$$

so

$$N_B = N_A^0 \frac{\lambda_A}{\lambda_B - \lambda_A} (e^{-\lambda_A t} - e^{-\lambda_B t}) + N_B^0 e^{-\lambda_B t} \quad (2)$$

Thus the disintegration rate of the daughter is given by

$$D_B = D_A^0 \frac{\lambda_B}{\lambda_B - \lambda_A} (e^{-\lambda_A t} - e^{-\lambda_B t}) + D_B^0 e^{-\lambda_B t}$$

If the parent has a much shorter half-life than the daughter, then

$$\lambda_A \gg \lambda_B \text{ and}$$

$$N_B = (N_A^0 + N_B^0) e^{-\lambda_B t} \quad \text{for } t \gg t_{1/2 A}. \quad (3)$$

This argument may be extended for a longer decay chain; thus if all the precursors of a species have relatively short half-lives, simple extrapolation of the disintegration rate of that species to $t = 0$ will give the total number of nuclei of all members of the chain.

If the parent has a longer half-life than the daughter, then $\lambda_A < \lambda_B$

and

$$N_B = N_A^0 \frac{\lambda_A}{\lambda_B - \lambda_A} e^{-\lambda_A t} \quad \text{for } t \gg t_{1/2 B}, \quad (4)$$

giving

$$D_B = D_A^0 \frac{\lambda_B}{\lambda_B - \lambda_A} e^{-\lambda_A t}.$$

Thus the activity of the parent may be determined from the activity of the

daughter

$$D_A^0 = \frac{\lambda_B - \lambda_A}{\lambda_B} D_B^0$$

$$\text{where } D_B^0 = D_B e^{\lambda_A t}$$

The cumulative yields of the decay chains leading to ^{95}Zr and ^{97}Zr were determined from the activity of the zirconium. The cumulative yield of the decay chain leading to ^{99}Mo was determined from the activity of the molybdenum, which was in turn derived from the observed activity of the daughter $^{99\text{m}}\text{Tc}$. The independent yields of ^{95}Nb and ^{97}Nb were in fact the combined yields of $^{95\text{m}}\text{Nb}$ plus $^{95\text{g}}\text{Nb}$ and of $^{97\text{m}}\text{Nb}$ plus $^{97\text{g}}\text{Nb}$. The metastable isomer in each case decays directly to the ground state with a relatively short half-life. For each species, the decay was studied by following the decrease in the rate of emission of only one γ -ray. The energies and abundances of these are given in Table I.

Table I

Energies and abundances of γ -rays observed.
(From Lederer et al, 1967)

nuclide	half-life	energy (keV)	abundance (per 100 disintegrations)
^{95}Nb	35 days	765	100
^{97}Nb	74 mins	665	98
^{95}Zr	65.5 days	765	49
^{97}Zr	17 hours	747	92
^{99}Mo	66.7 hours	140	87

The γ -ray spectra were observed with a lithium-drifted germanium detector and a multi-channel analyser. The work was begun with an Ortec 30 cm³ model 8001-0536 detector, an Ortec 118A pre-amplifier, and an Ortec 440 multimode amplifier. Later an Ortec 438 base-line restorer was included. For the niobium and molybdenum work a 40 cm³ model 8101-0725 detector and a 120-2B pre-amplifier were used. The analyser was a Victoreen Scipp 1600-channel model SD-2P. The annihilation radiation of the positrons emitted by the ⁶⁴Cu was observed with a 3"x3" NaI(Tl) crystal and an RIDL model 34-12B 400-channel analyser.

The γ -rays emitted by a collection of excited nuclei undergoing a given transition will be recorded by a multi-channel analyser of low conversion gain (keV/channel) in any of several channels, rather than in precisely one. Thus it is necessary to find the total number of events recorded in this group of channels by adding together the individual records. Since this total record includes background radiation as well as the photo peak, the background must be subtracted.

In the case of the γ -spectrum analysis carried out with the Ge(Li) detectors and the 1600-channel analyser, the contents of several channels to either side of a peak were summed to give an estimate of the background under the peak. Usually the peaks were symmetric, and a group of half the number of channels needed to span a peak was taken for background on either side (Figure 7). When a peak was obviously asymmetric, a reasonable estimate of the background could be made by adjusting the extent of the groups of background channels to be complementary to the asymmetry.

The resolution of the Ge(Li) detectors was about 0.4% (full-width at half-maximum) in the energy range of interest. The conversion gain of the

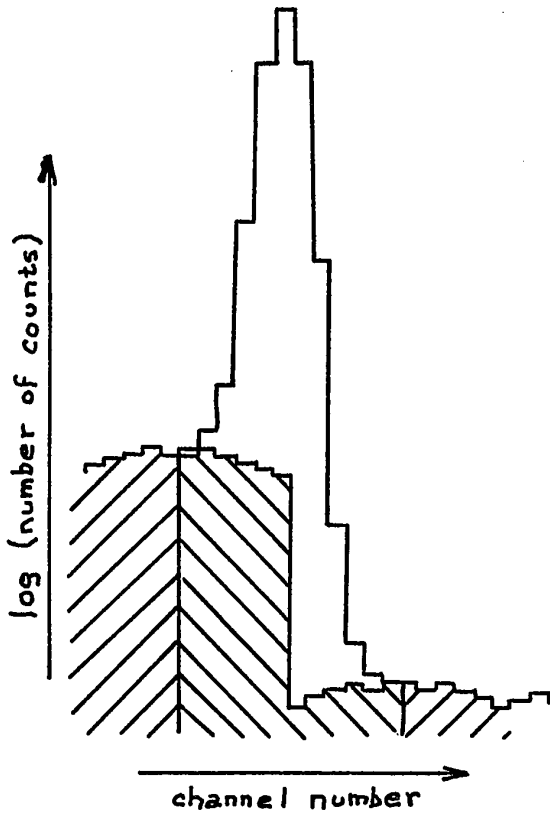


Figure 7.
A peak in a γ -ray spectrum as recorded by a Ge(Li) detector and 1600-channel analyser. The shaded area under the peak is the estimated background, obtained by reflecting the shaded area to either side of the peak.

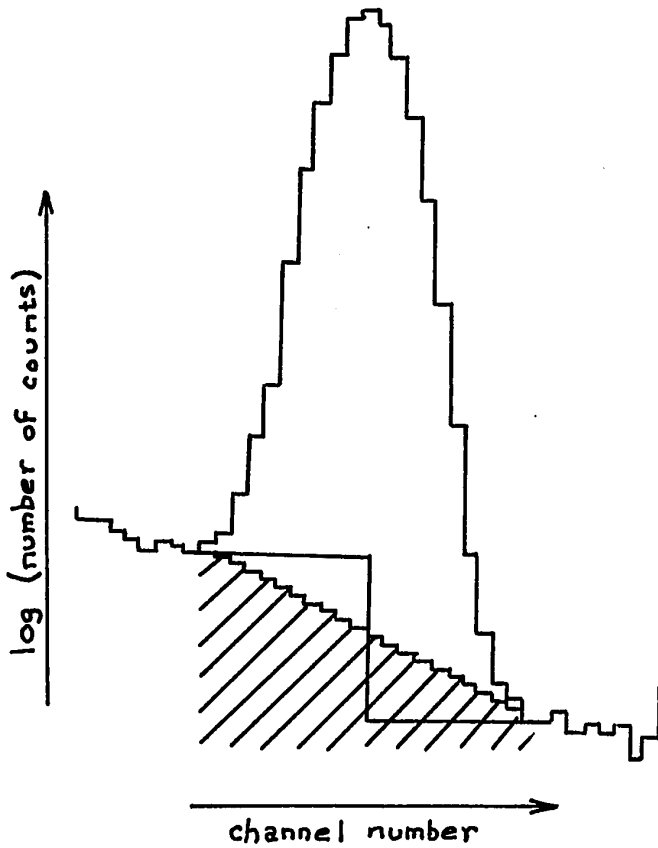


Figure 8.
The annihilation radiation peak of ^{64}Cu . The shaded area is the estimated background.

analyser was set at about 0.7 keV/channel. The resolution of the NaI crystal used to detect the radiations of the ^{64}Cu samples was about 8%, and the conversion gain of the system 7 keV/channel. Here a different approach was used to estimate the background under the peak. The background included in each channel across the peak was taken to be equal to the average of the number of events recorded in the first channel to either side of the peak. This could of course be interpreted as equivalent to a step function, and so similar to the background in the case of the γ -ray analysis, or as a steadily decreasing function of channel number, as shown in Figure 8.

The rate at which γ -rays are emitted by an active source is simply found from the rate at which they are collected by a detector of known efficiency. If a sample is observed for a time which is short relative to its half-life, then the average activity over the interval may be taken as the activity at the mid-point of the interval, since the expression $A = A^0 e^{-\lambda t}$ can be approximated by $A = A^0(1 - \lambda t)$. Rigorously, the average activity is equal to the activity at a time

$$\tau = -\frac{1}{\lambda} \ln \left(\frac{1}{\lambda \Delta t} (1 - e^{-\lambda \Delta t}) \right)$$

after the beginning of the interval Δt . It is clearly more convenient to use very active samples to allow short counting intervals and the subsequent approximation of $\tau = \frac{1}{2} \Delta t$.

In the present work the count rates of the chosen transition for each species were observed at various times and the value of the count rate at the time of chemical separation or at the end of bombardment obtained by extrapolation. The disintegration rate and hence the number of excited nuclei initially present was derived from the extrapolated count rate, the detector efficiency,

the branching ratio of the transition, and the chemical yield (or fraction of recovery). The extrapolation of the decay curve was performed by fitting a function of the form

$$\ln c = \ln c^0 - \lambda t \quad \text{where } c \text{ is the count rate}$$

to the original data. A linear least-squares fit was used, noting that

$$\Delta(\ln c) \approx \frac{\Delta c}{c}$$

and, beyond that correction, allowing all points equal weight.

Calculation of Cross Sections

The production cross sections for the various fission products were calculated by a comparison of the actual yields of the fission products to the actual yield of ^{64}Cu from the monitor reaction $^{65}\text{Cu}(p,pn)^{64}\text{Cu}$. The cross sections for the monitor reaction are given in Table II.

Table II

Cross sections for the monitor reaction $^{65}\text{Cu}(p,pn)^{64}\text{Cu}$
(From Meghir, 1962)

proton energy (MeV)	cross section (mb)
20	260
30	390
40	260
50	210
60	180
72	160
85	140

While a target is in the cyclotron, assuming that the intensity of the beam is constant, the rate of formation of the product of a reaction is given by

$$\begin{aligned}
 - \frac{d N_p}{d t} &= \text{rate of production} - \text{rate of decay} \\
 &= I n_T \sigma_p - \text{rate of decay}
 \end{aligned}$$

where I is the beam intensity

n_T is the number of target nuclei

σ_p is the cross section for the reaction.

Thus
$$N_p = \frac{I n_T \sigma_p}{\lambda_p} (1 - e^{-\lambda_p t}) \quad (5)$$

at any time during the irradiation,

and so
$$D_p^b = I n_T \sigma_p (1 - e^{-\lambda_p t_b})$$

where t_b is the duration of the bombardment

D^b is the disintegration rate at the end of the bombardment.

If t_b is small relative to the half life, this becomes

$$D_p^b = I n_T \sigma_p \lambda_p t_b. \quad (6)$$

Thus, denoting the monitor by M and the product of the monitor reaction by M^* ,

$$\frac{D_p^b}{D_{M^*}^b} = \frac{I n_T \sigma_p \lambda_p t_b}{I n_M \sigma_{M^*} \lambda_{M^*} t_b}$$

and since the target and monitor are mixed together and subjected to the same beam of protons for the same time, this gives

$$\sigma_P = \sigma_{M^*} \frac{D_P^b n_M \lambda_{M^*}}{D_{M^*} n_T \lambda_P} \quad (7)$$

The terms in this expression are easily calculated as follows:

$$D^b = \frac{\text{extrapolated initial count rate}}{\text{efficiency of detector}} \cdot \frac{1}{\text{branching ratio}} \cdot \frac{1}{\text{chemical yield}}$$

$$n_M = (\text{weight of CuO})(\text{fraction of Cu in CuO})(\text{fraction of } ^{65}\text{Cu} \\ \text{in Cu})(\text{Avogadro's number})/(\text{atomic weight of Cu})$$

$$n_T = (\text{weight of } ^{233}\text{U}_3\text{O}_8)(\text{fraction of } ^{233}\text{U in } ^{233}\text{U}_3\text{O}_8)(\text{Avogadro's} \\ \text{number})/(\text{atomic weight of } ^{233}\text{U}).$$

In the calculations of the cumulative cross sections of $^{95}\text{Zr}(t_{1/2} = 65.5 \text{ day})$, $^{97}\text{Zr}(t_{1/2} = 17 \text{ hr})$, and $^{99}\text{Mo}(t_{1/2} = 66.7 \text{ hr})$ the approximation inherent in equation (6) was considered valid for the fission product species as well as for the monitor, and equation (7) was applied. In the calculations of the independent cross sections it was necessary to consider the contribution to the total yield from the decay of precursors during the bombardment or before chemical separation. Certainly the contribution of $^{95}\text{Zr}(65\text{-day})$ to the yield of ^{95}Nb during a ten-minute bombardment or a thirty-five minute interval before separation is negligible. In the case of the growth of ^{97}Nb from $^{97}\text{Zr}(17\text{-hour})$, the contribution made during the bombardment was neglected, but that made during the following interval before the first precipitation of niobic acid was taken into account.

At the end of bombardment, the number of ^{97}Nb nuclei formed directly from fission is given by

$$N_B^b = I n_T \sigma_B (1 - e^{-\lambda_B t_b}).$$

At the time of chemical separation, the number of these nuclei remaining is given by $N_B^s = N_B^b e^{-\lambda_B t_s}$ where t_s is the time interval from the end of bombardment to separation.

During this same interval, some of the ^{97}Zr present will decay to ^{97}Nb , making the total number of ^{97}Nb nuclei at the time of separation

$$N_B^s = I n_T \sigma_B (1 - e^{-\lambda_B t_b}) e^{-\lambda_B t_s} + N_A^b \frac{\lambda_A}{\lambda_B - \lambda_A} (e^{-\lambda_A t_s} - e^{-\lambda_B t_s}) \quad (8)$$

From equation (7)

$$N_A = \frac{n_T \sigma_A}{n_M \sigma_{M^*}} N_{M^*}$$

Substituting this into equation (8) and noting again that the target and monitor are subjected to the same beam of protons gives

$$\sigma_B = \frac{\lambda_B}{(1 - e^{-\lambda_B t_b})} \cdot \frac{t_b}{(e^{-\lambda_B t_s})} \left\{ \frac{N_B^s n_M \sigma_{M^*}}{N_{M^*} n_T} - \sigma_A \frac{\lambda_A}{\lambda_B - \lambda_A} (e^{-\lambda_A t_s} - e^{-\lambda_B t_s}) \right\} \quad (9)$$

Errors

The total error in the cross-section is given as the sum of the squares of the contributing experimental errors. The error in the initial disintegration rate was between 2% and 9%. The error in the weighing of the target was taken as $\pm 2\%$, that of the chemical determination $\pm 5\%$, and the error in the efficiency calibration of the detector $\pm 10\%$. The uncertainty in the time of separation of the niobium was about 7%; the error in the duration of the bombardment was negligible. The error introduced by the assumption that $N_B = (N_A^o + N_B^o) e^{-\lambda_B t}$ is negligible in the case of ^{97}Nb (74-minute ground state and 1-minute isomer) and at most 12% for ^{95}Nb (35-day ground state and 90-hour isomer). This figure represents the extreme situation that all the ^{95}Nb is created in the metastable state.

Chapter 3

Results

The formation cross sections of the various species studied are given in Table III and the excitation functions are shown in Figures 9 - 13.

The peak of the excitation function of ^{97}Nb ($N/Z = 1.366$) occurs at about 40 MeV bombarding energy. This does not fall on the curve of the peaking energy as a function of N/Z derived from the excitation functions of cesium isotopes produced from the fission of ^{233}U (Figure 5). Khan (1968) also noted that the peaking energies of the excitation functions of yttrium isotopes produced from the fission of ^{235}U and ^{238}U do not lie on the cesium curves.

Charge dispersion curves as functions of N/Z were constructed directly from the cross-sections, assuming that the mass-yield curve is flat for $95 \leq A \leq 101$, that N/Z_p does not vary over this mass range, and that the dispersions are symmetric. The right-hand (neutron excessive) side of each curve is defined by the cumulative chain yields, as shown by Friedlander *et al.*, and the assumed symmetry. The results are shown in Figures 14 - 19. It should be noted that these curves are given in the form $\ln \sigma = f(N/Z)$. Figure 20 shows one of the curves recast in the form $\sigma = f(N/Z)$, illustrating the asymptotic tails which are a direct result of the exponential nature of the original curves.

Z_p was easily calculated from the N/Z value at the peak of the charge dispersion, since $Z = A/(N/Z + 1)$. (A) was taken as the mass number, to the nearest 0.2, of the niobium isotope with N/Z closest to N/Z_p . Z_A was calculated from the Z_A function of Coryell (1953). The full-width at half-maximum was calculated in Z units by converting the N/Z values at the half-

Table III

Formation cross sections (mb).

proton energy (MeV)	^{95}Nb (indep)	^{97}Nb (indep)	^{95}Zr (cum)	^{97}Zr (cum)	^{99}Mo (cum)
20		2.1 ± 0.3	40 ± 5	45 ± 6	27 ± 3
30	0.47 ± 0.06	6.0 ± 0.8	32 ± 4	34 ± 4	48 ± 6
40	2.1 ± 0.3	16 ± 2	73 ± 10	75 ± 10	95 ± 13
50	0.47 ± 0.06	10 ± 1	45 ± 6	47 ± 6	61 ± 7
60	1.2 ± 0.15	6.7 ± 0.9	40 ± 5	39 ± 5	55 ± 6
72	2.7 ± 0.4	9.8 ± 1.4	52 ± 6	50 ± 6	52 ± 6
85	3.6 ± 0.5	11 ± 1.9	44 ± 6	42 ± 6	51 ± 8

maximum points to Z values. The mass number determined from the value of N/Z_p was used here as well, since the result appeared to be insensitive to the choice of A within the range spanned by these curves. The results of these calculations are given in Table IV, and compared to those of Khan et al in Table V and Figure 21.

The charge dispersion curves are drawn empirically to minimize the sum of the squares of the differences between the experimental and interpolated cumulative yields. Attempts were made to find a computable function, σ (or $\ln \sigma$) = $f(N/Z)$, governing the form of the dispersion curves. Various functions were constructed employing the parameters N/Z_p , σ_p (the maximum value of σ), and a width parameter; none generated curves having a reasonable fit to the data at all energies.

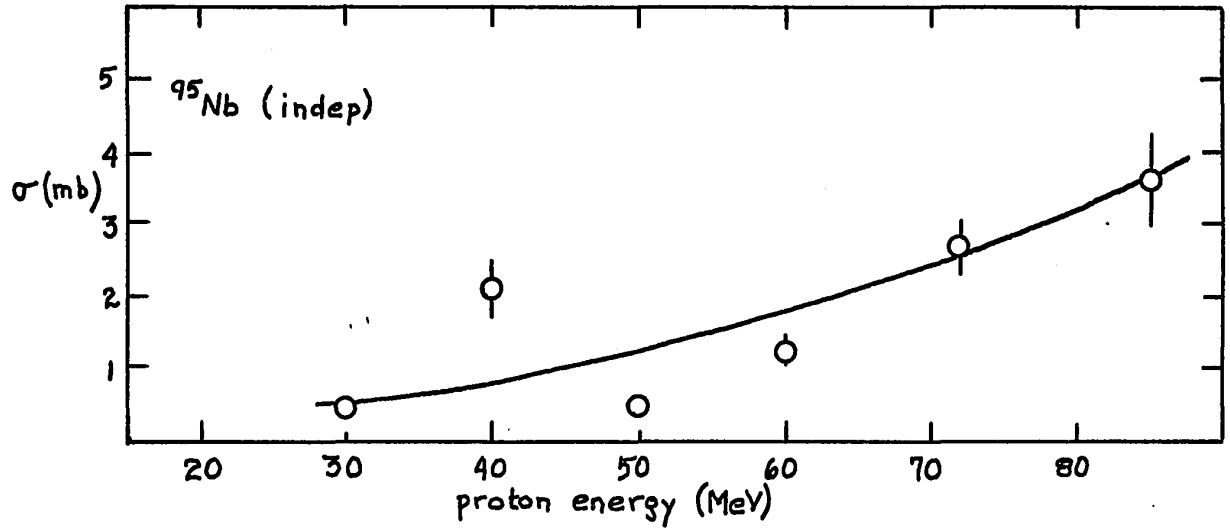


Figure 9. The excitation function of ^{95}Nb (independent yield).

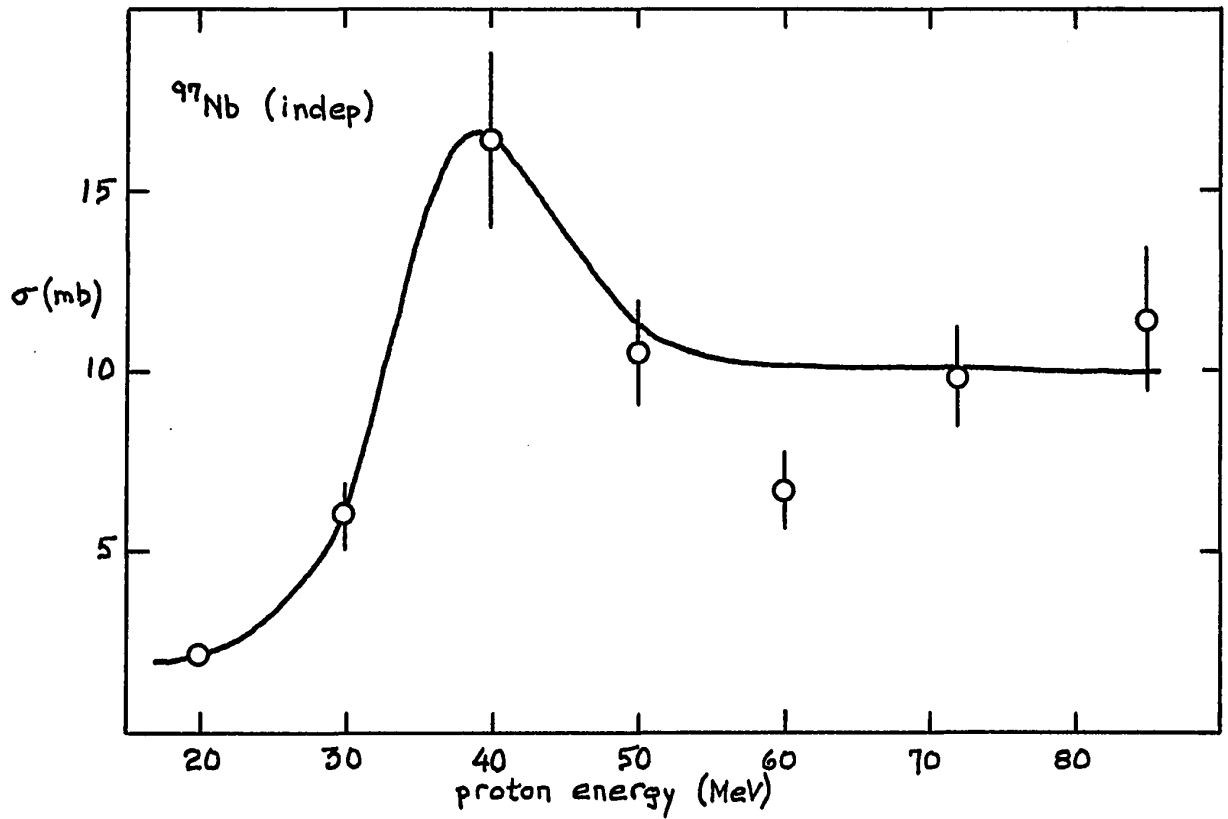


Figure 10. The excitation function of ^{97}Nb (independent yield).

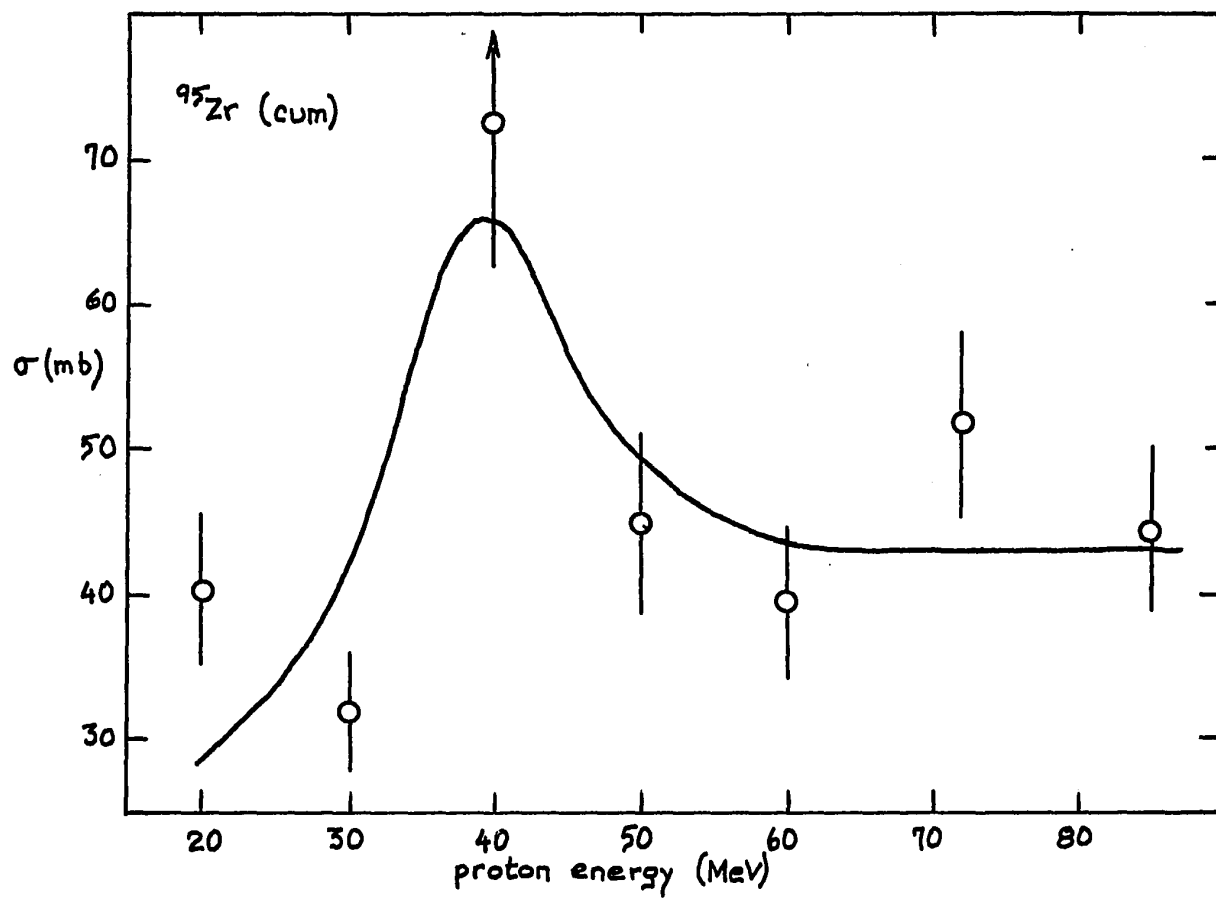


Figure 11. The excitation function of ^{95}Zr (cumulative yield).

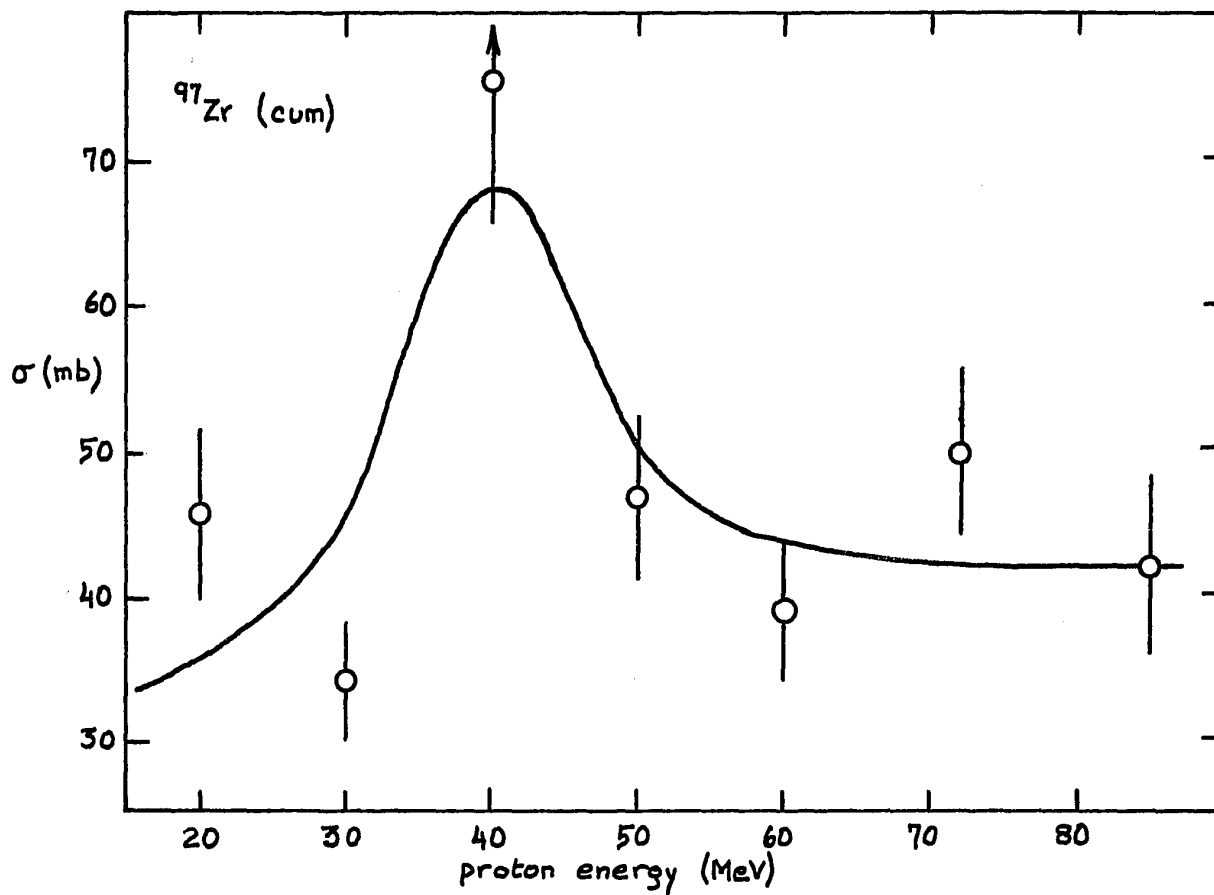


Figure 12. The excitation function of ^{97}Zr (cumulative yield).

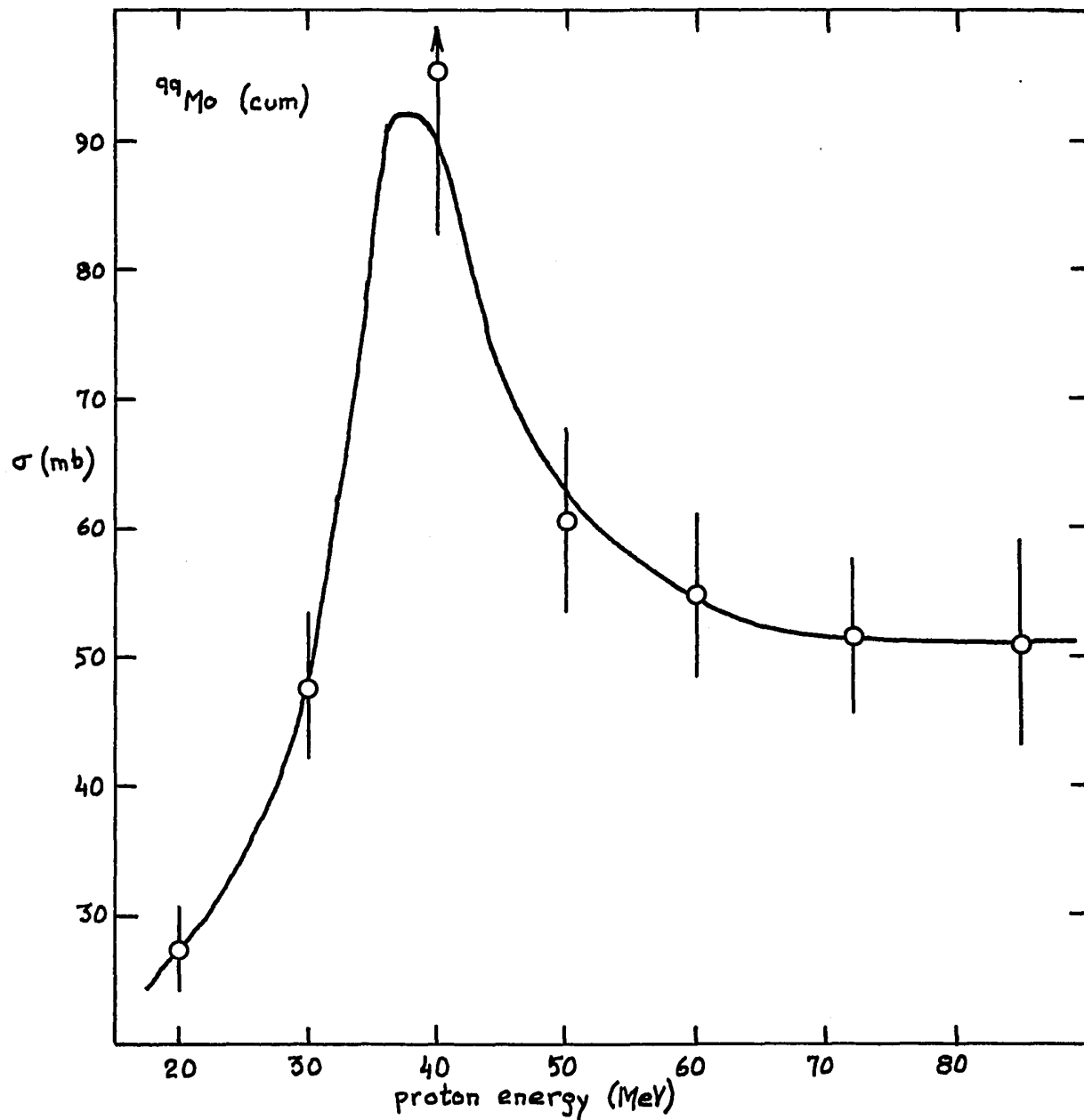


Figure 13. The excitation function of ^{99}Mo (cumulative yield).

Figures 14 - 19

Charge dispersion curves at bombarding energies 30 - 85 MeV. The right-hand sides of the curves were drawn such that the interpolated cumulative yields approximate the experimental values.

proton energy (MeV)	cumulative yields (mb)					
	⁹⁵ Zr		⁹⁷ Zr		⁹⁹ Mo	
	interp.	exptl	interp.	exptl	interp.	exptl
30	38.1	32.0	34.4	34.0	40.6	47.7
40	83.3	72.6	69.6	75.4	89.2	95.4
50	52.5	45.0	42.8	46.7	55.2	60.6
60	43.9	39.6	39.5	38.9	48.0	54.8
72	50.8	51.8	42.5	49.8	54.2	51.7
85	48.0	44.4	38.2	41.9	51.7	51.0

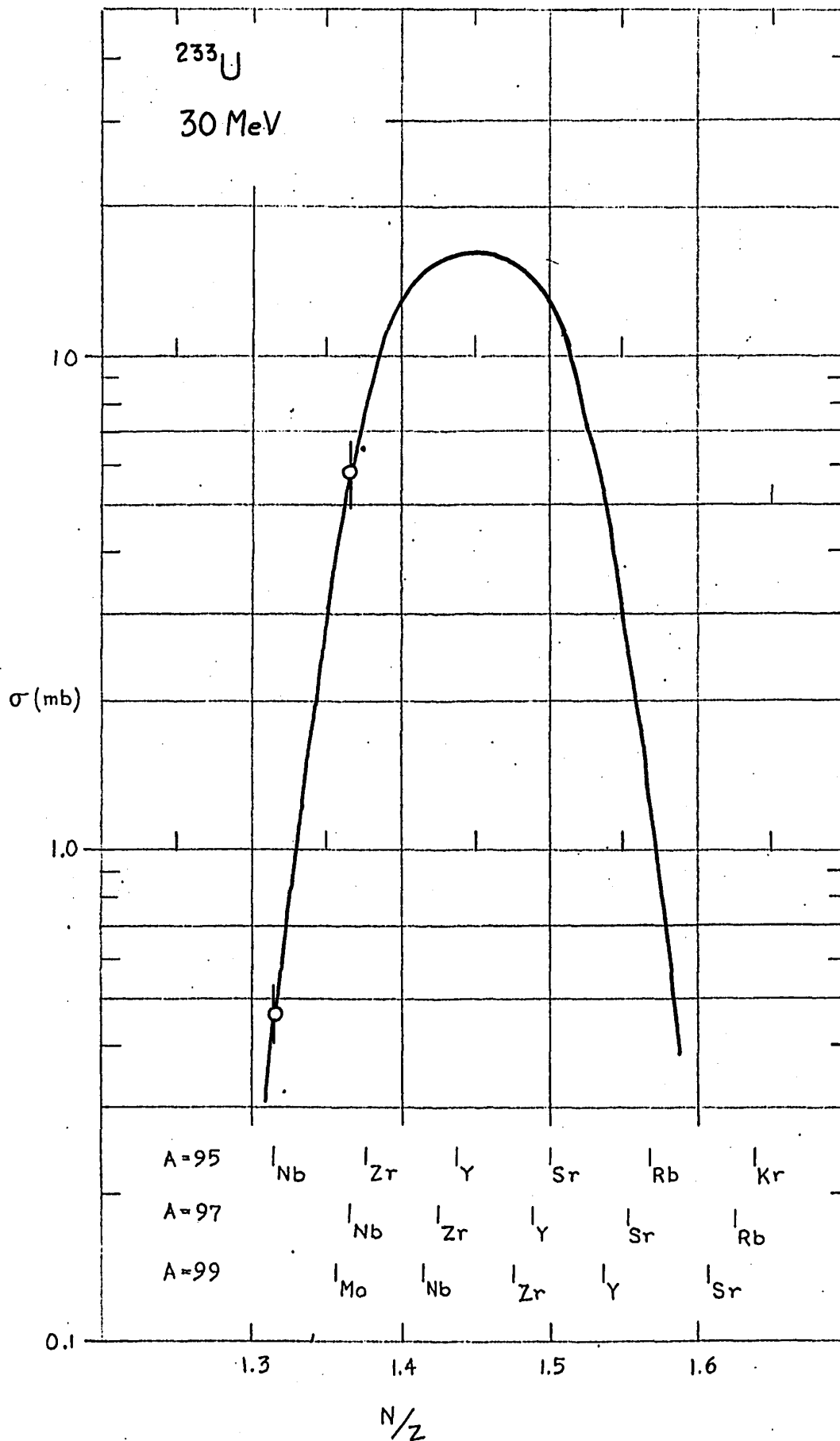


Figure 14. Charge dispersion at 30 MeV bombardment energy.

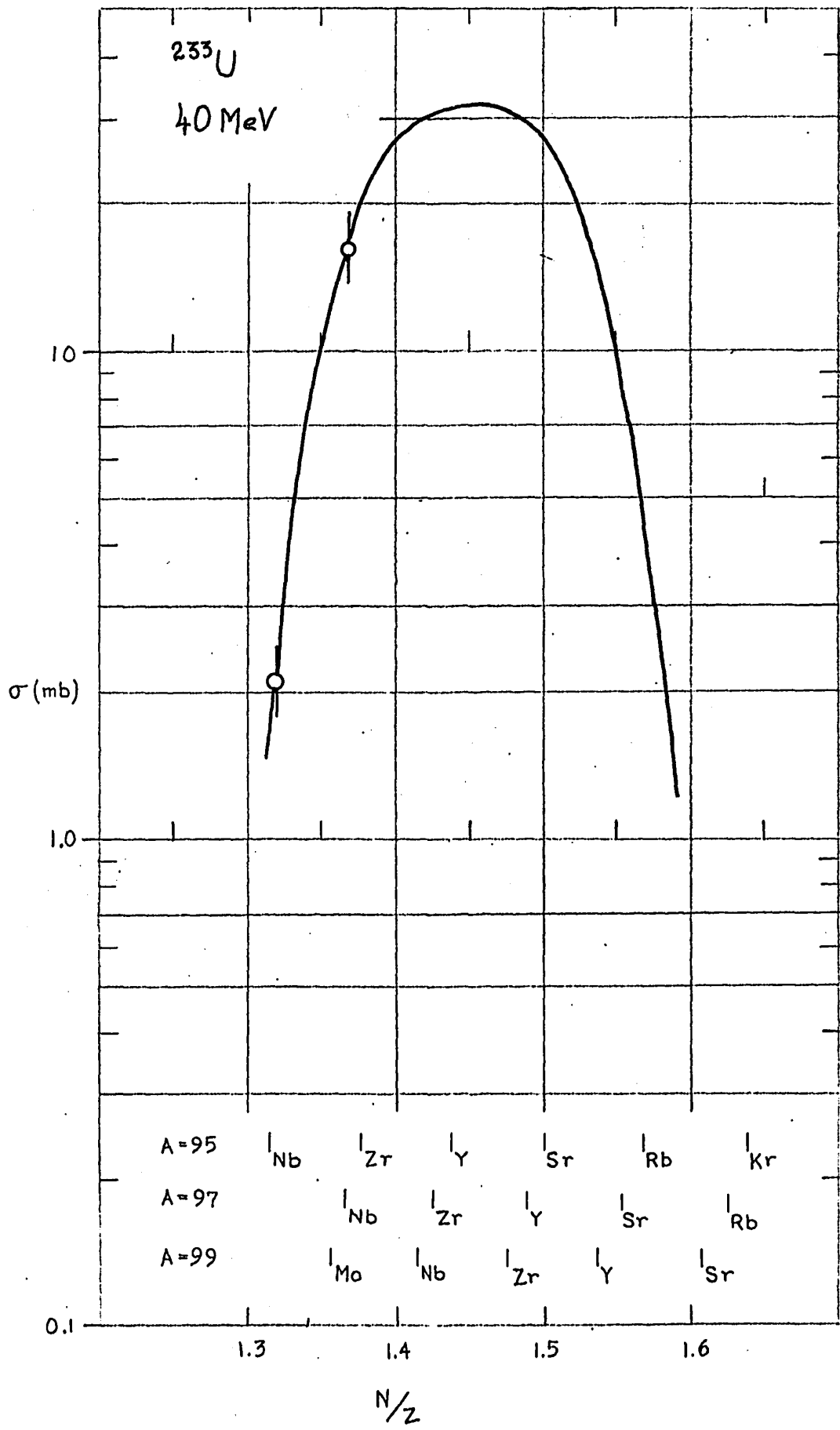


Figure 15. Charge dispersion at 40 MeV bombardment energy.

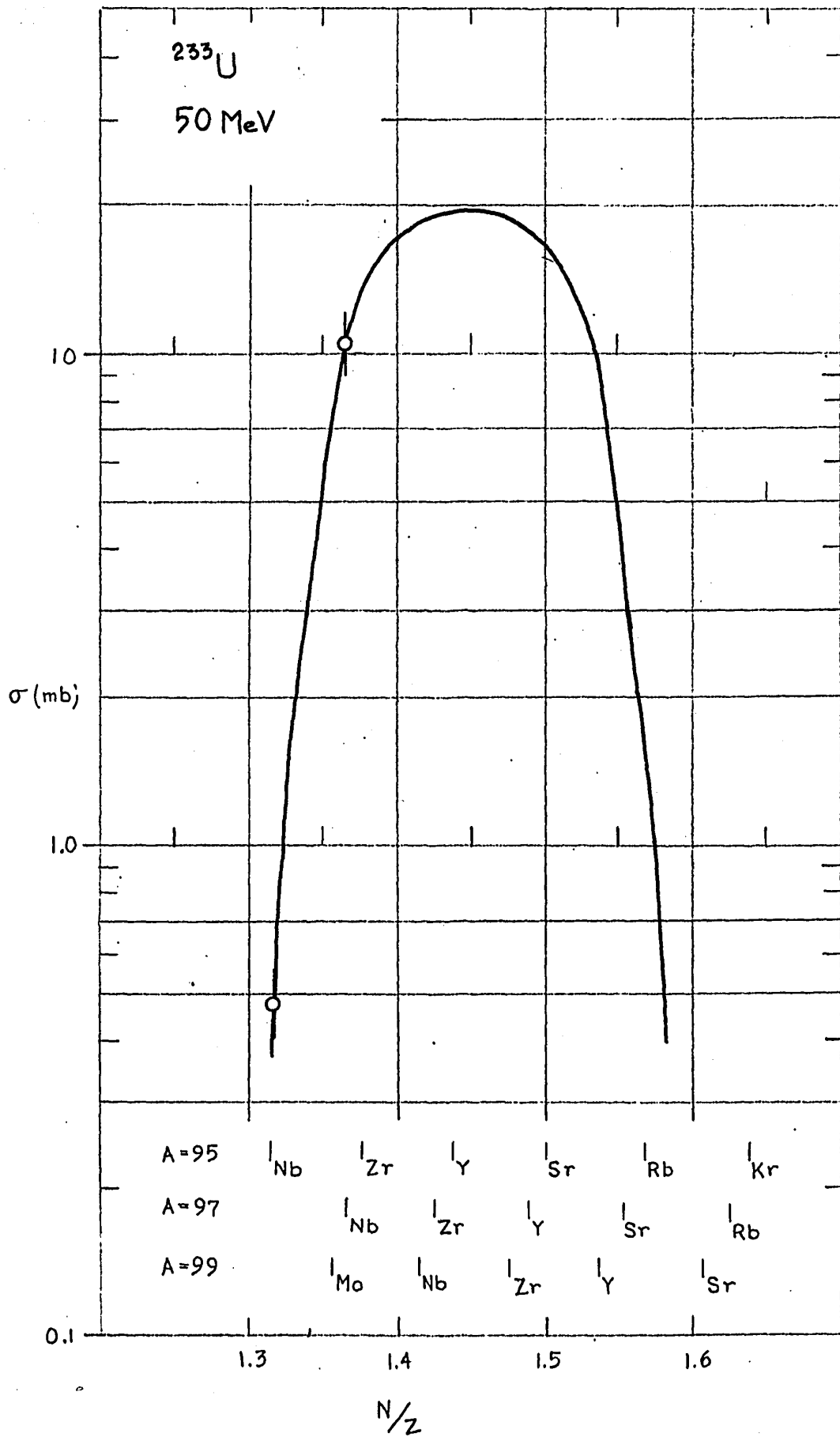


Figure 16. Charge dispersion at 50 MeV bombardment energy.

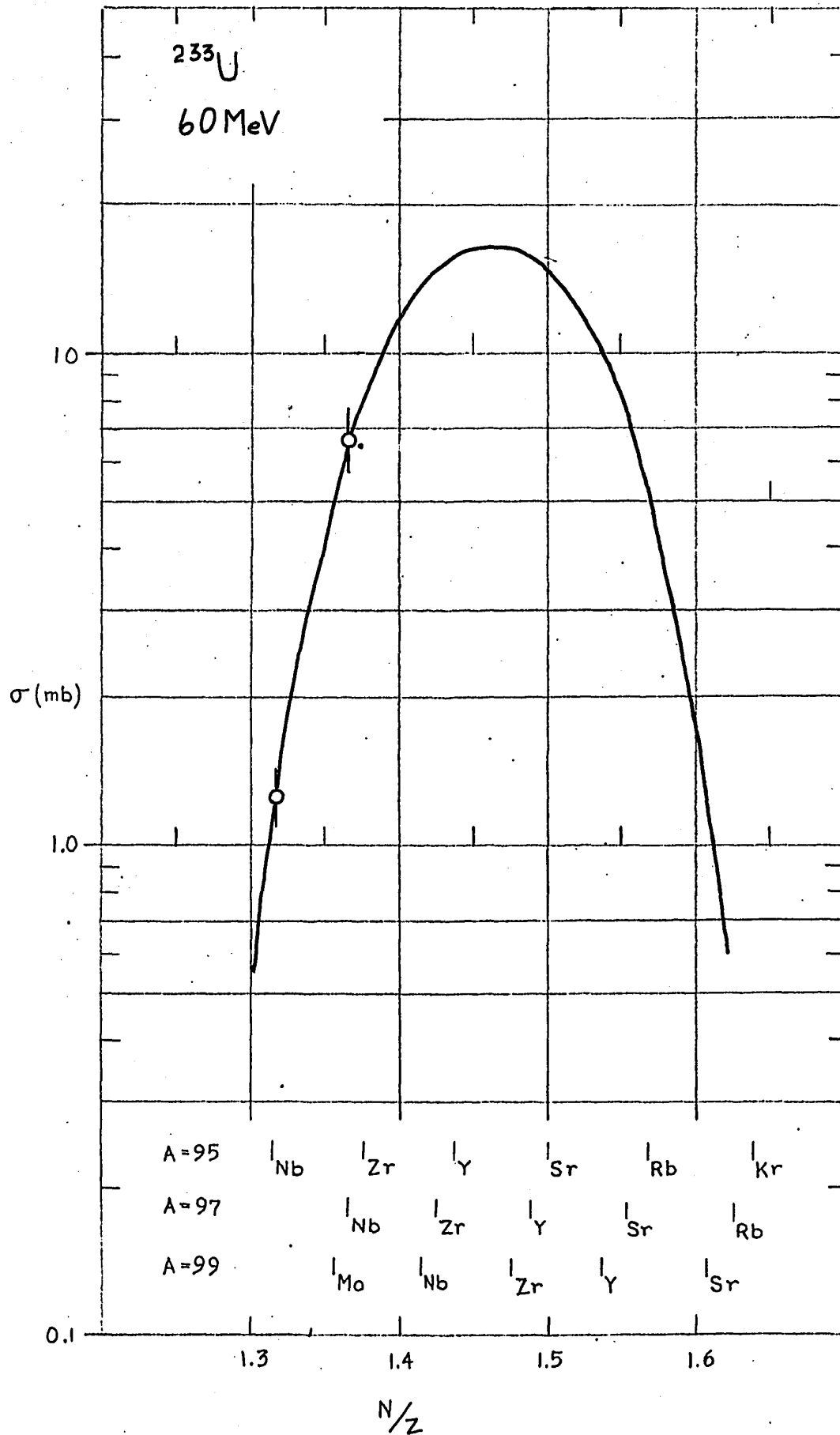


Figure 17. Charge dispersion at 60 MeV bombardment energy.

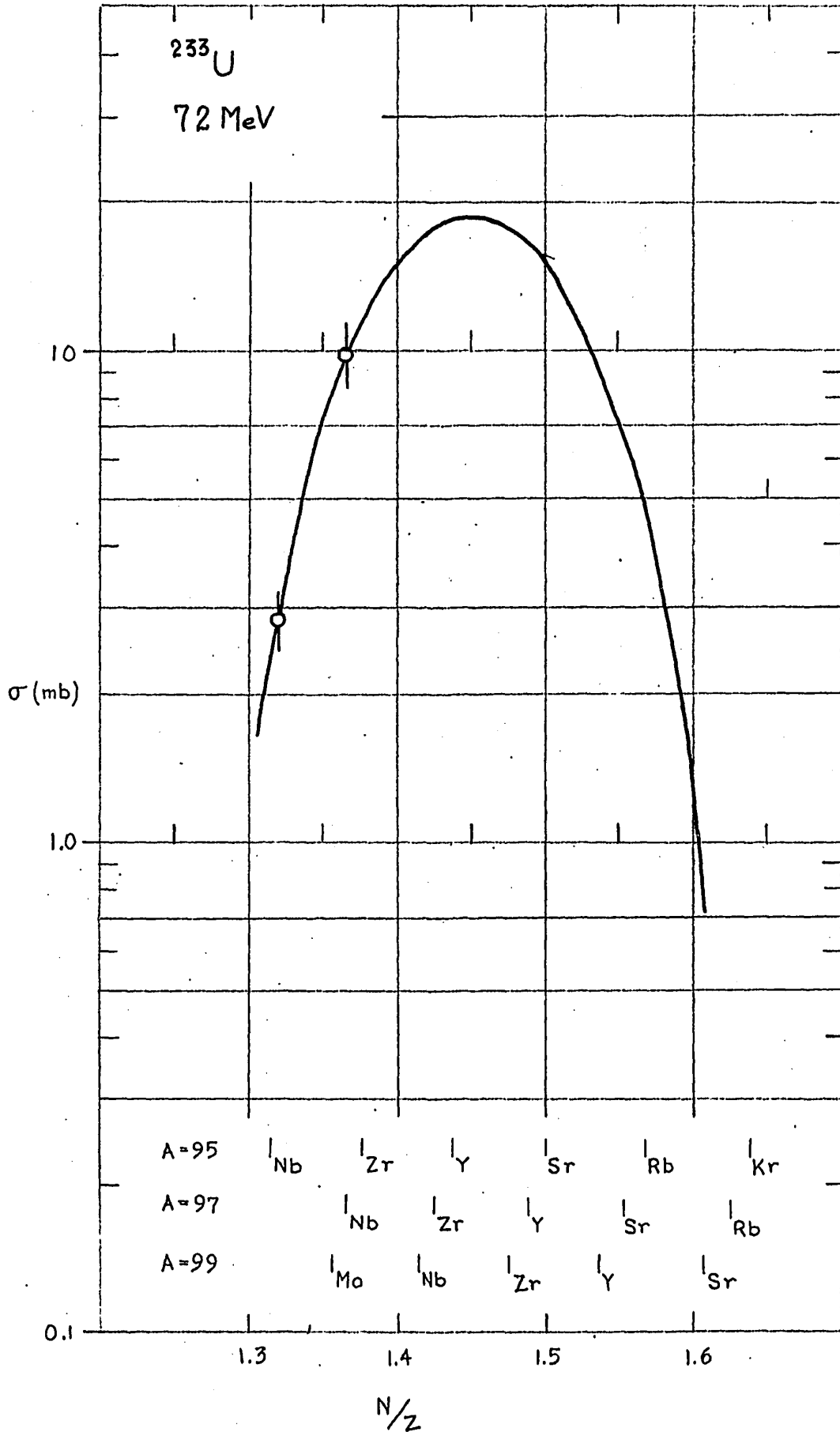


Figure 18. Charge dispersion at 72 MeV bombardment energy.

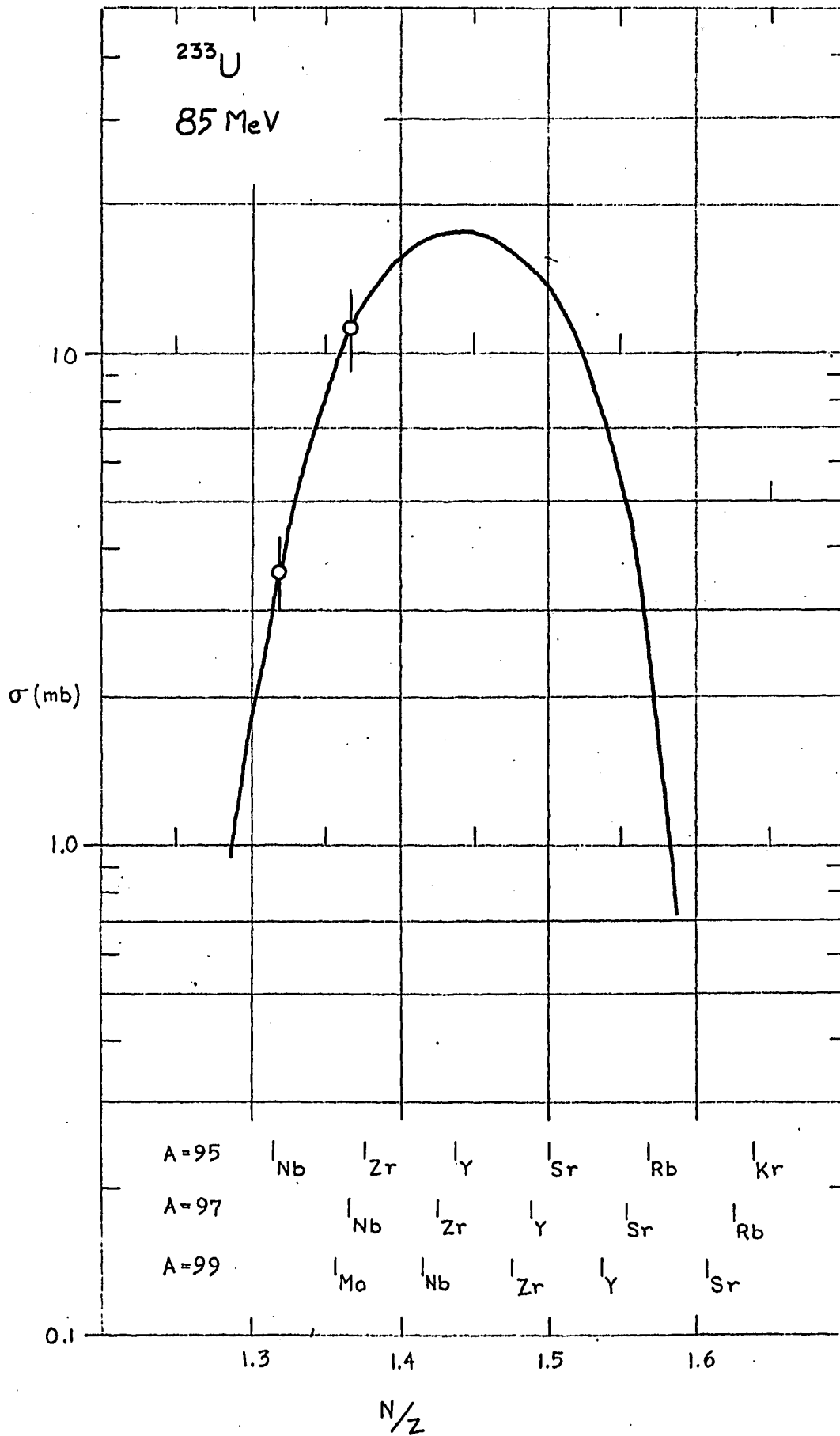


Figure 19. Charge dispersion at 85 MeV bombardment energy.

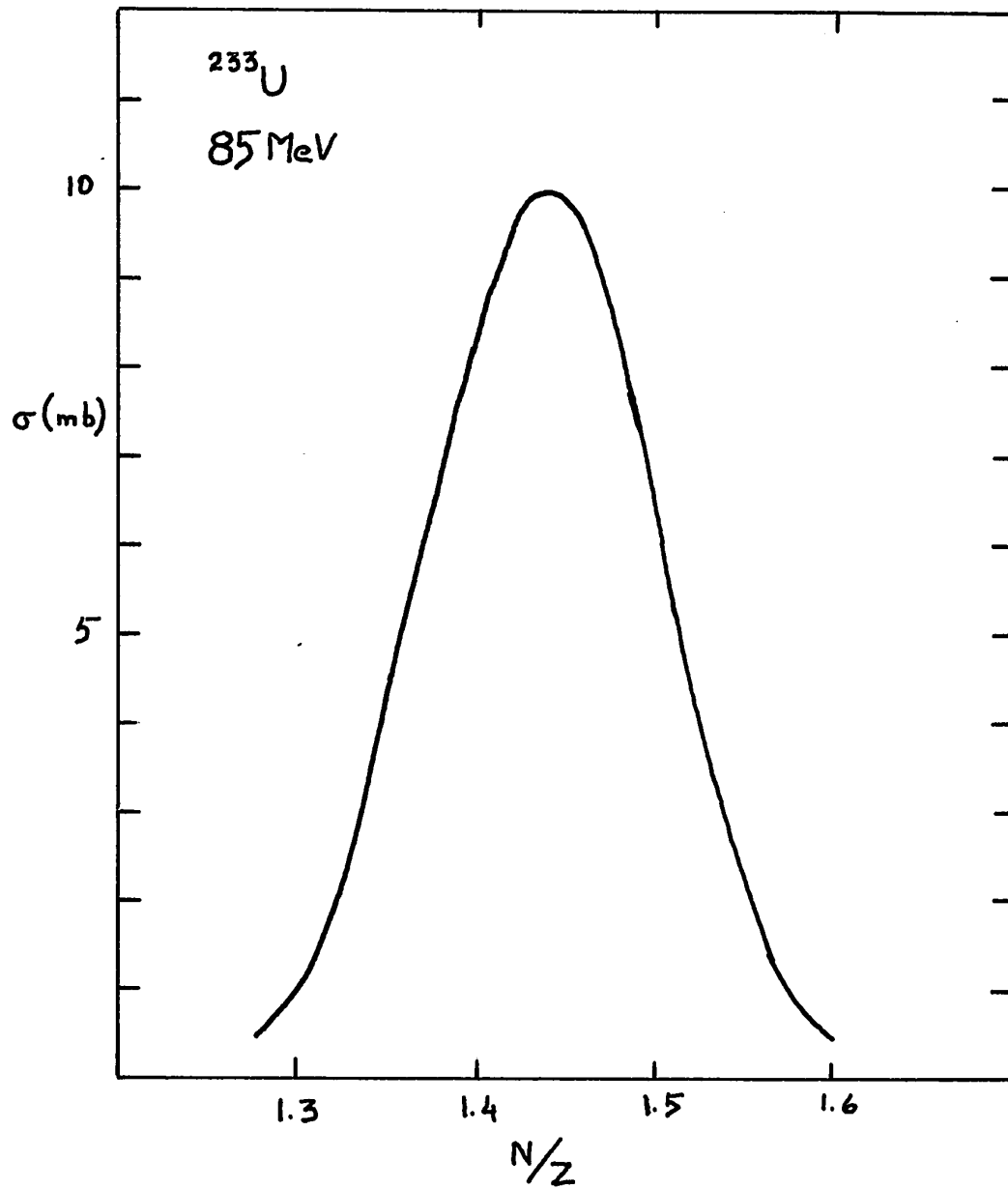


Figure 20. Charge dispersion at 85 MeV bombardment energy (σ vs N/Z).

Table IV

Parameters of charge dispersion curves for ^{233}U .

proton energy (MeV)	full-width at half-maximum		peak position		
	$\Delta N/Z$	ΔZ	N/Z_p	Z_p	$Z_A - Z_p$
30	0.145	2.4	1.450	40.98	2.94
40	0.170	2.8	1.450	40.98	2.94
50	0.174	2.9	1.450	40.98	2.94
60	0.175	2.9	1.465	40.97	3.18
72	0.174	2.9	1.450	40.98	2.94
85	0.180	3.0	1.440	40.98	2.78

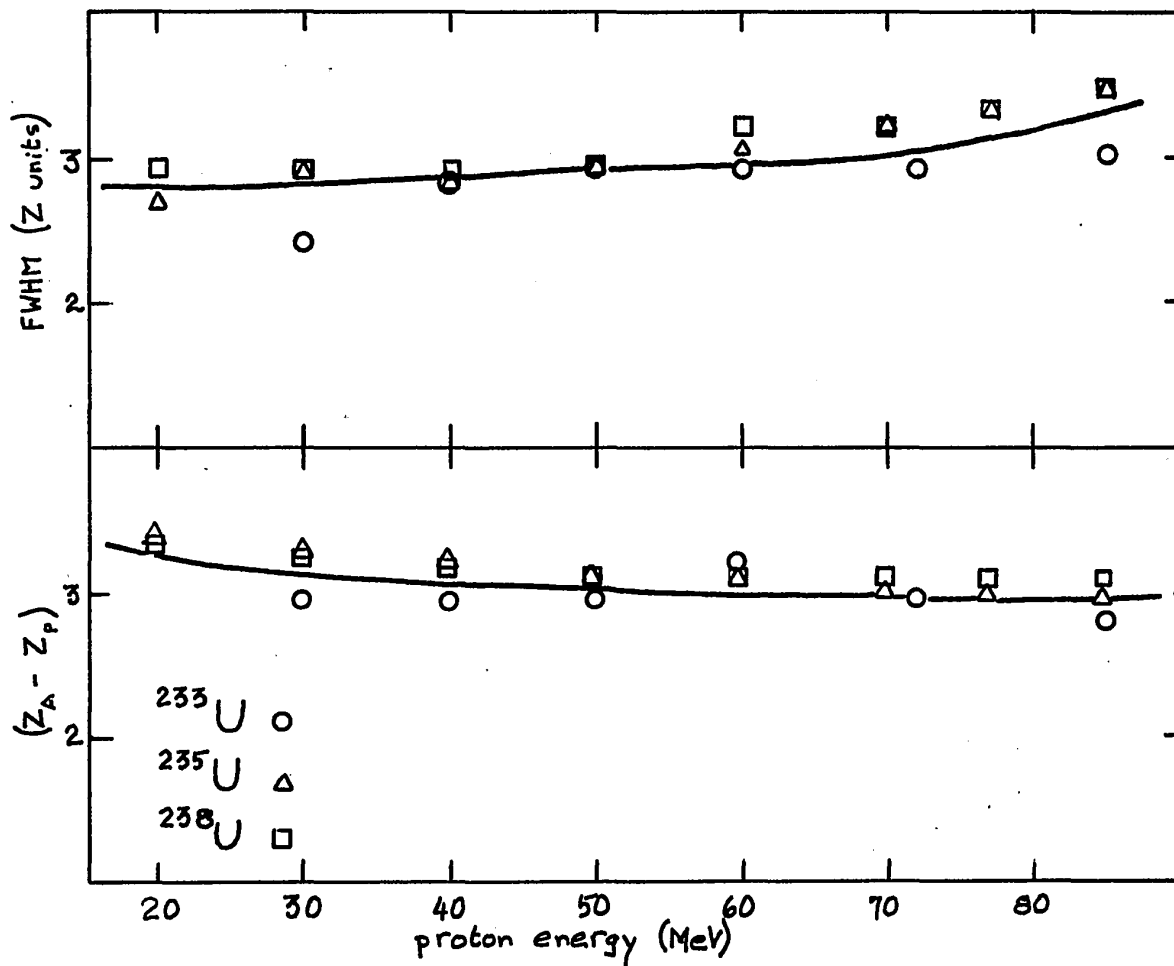


Figure 21. The full-width at half-maximum of the charge dispersion curves and the displacement of the most probable charge from stability for the fission of ^{233}U , ^{235}U , and ^{238}U .

Table V

Parameters of charge dispersion curves for
 ^{233}U , ^{235}U , and ^{238}U .

proton energy (MeV)	FWHM (Z)			$(Z_A - Z_p)$		
	^{233}U	^{235}U	^{238}U	^{233}U	^{235}U	^{238}U
20		2.7	2.9		3.42	3.34
30	2.4	2.9	2.9	2.94	3.27	3.25
40	2.8	2.8	2.9	2.94	3.23	3.18
50	2.9	2.9	2.9	2.95	3.13	3.10
60	2.9	3.1	3.2	3.18	3.07	3.10
70		3.2	3.2		3.02	3.10
72	2.9			2.94		
77		3.3	3.3		3.02	3.10
85	3.0	3.4	3.4	2.78	2.95	3.10

Chapter 4

Discussion

The shift of Z_p towards Z_A with increasing energy and the slight broadening of the charge dispersions observed in this work are trends observed and discussed in previous charge dispersion studies of both heavy and light fragments in this energy range. However, in the heavy-mass region the displacement from stability shows a strong dependence on the nature of the target, while the present work supports Khan's observation that in the light-mass region there is no such dependence over a set of isotopic targets.

The strong target dependence of the charge dispersion in the heavy products of asymmetric fission and the lack of dependence in the light products can be resolved by the view that the similarity of the light products in fact forces the heavy products to absorb all the variation introduced by differing targets. To test the feasibility of this explanation, the results of Davies and Yaffe for the fission of ^{238}U , of Tomita and Yaffe for ^{233}U , and of Saha et al for ^{235}U were compared. The comparison was carried out only for bombarding energies of 20 to 50 MeV, since the compound nucleus mechanism may be assumed in this range. The three studies were all based on the fission yields of various cesium isotopes, and the mass numbers of those nearest the peaks of the charge dispersion curves fall within a narrow range ($136 \leq A \leq 140$).

The differences among the target nuclei are simply in the number of neutrons; ^{235}U has two more neutrons and ^{238}U five more, than ^{233}U . Thus the excited compound nuclei differ only in the number of constituent neutrons. The average fissioning nucleus was calculated for each target at each energy. These are given in Table VI, along with $\bar{\nu}_{\text{pf}}$, the average number of neutrons emitted before fission. These average fissioning nuclei were calculated from

Table VI

Neutron emission characteristics of the compound nucleus and the heavy fragment for the proton-induced fission of ^{233}U , ^{235}U , and ^{238}U . The values in parentheses were interpolated from the original results.

proton energy (MeV)	average fissioning nucleus (mass number)	$\bar{\nu}_{\text{pf}}$	E^* (MeV)	ν_{h}	N/Z_{p}	Z_{p}	A_{h}
20	^{233}U	233.81	24.11		1.480	54.84	136
				0.19			
				0.82			
	^{235}U	235.65	24.76		1.500		137.10
				0.35			
				1.78			
	^{238}U	238.28	25.22		1.550		139.84
				0.72			
				1.66			
30	^{233}U	233.81	34.06		1.475	54.95	136
				0.19			
				1.16			
	^{235}U	235.64	34.72		1.484		136.50
				0.36			
				2.50			
	^{238}U	238.20	35.18		(1.534)		139.24
				2.32			
40	^{233}U	233.81	44.02		(1.470)	55.06	136
				0.19			
				1.50			
	^{235}U	235.64	44.67		1.473		136.16
				0.36			
				3.22			
	^{238}U	238.17	45.15		(1.521)		138.81
				0.83			
				2.98			
50	^{233}U	233.81	53.98		1.466	55.15	136
				0.19			
				1.84			
	^{235}U	235.64	54.63		1.463		135.83
				0.36			
				3.93			
	^{238}U	238.16	55.10		1.512		138.54
				0.84			
				3.64			

the data of Huizenga and Vandenbosch (1962), which are arranged to give Γ_n / Γ_f (the probability of neutron emission divided by that of fission) as a function of Z and A , assuming each neutron carries away 10 MeV of excitation energy. It was necessary to assume that Γ_n / Γ_f is not dependent on excitation energy over the range covered by Huizenga and Vandenbosch and the charge dispersion studies (8 - 55 MeV). The difference among the fissioning nuclei at each bombarding energy is still one of neutron content, but the differences grow smaller at higher energies.

McHugh and Michel (1968) proposed that the rate of neutron emission by the fragments could be determined from the dependence of Z_p on the excitation energy.

Since
$$\left(\frac{\partial Z_p}{\partial E} \right)_A = - \left(\frac{\partial Z_p}{\partial A} \right)_E \left(\frac{\partial A}{\partial E} \right)_{Z_p}$$

and
$$\left(\frac{\partial A}{\partial E} \right)_{Z_p} = - \left(\frac{\partial \bar{\nu}}{\partial E} \right)_{Z_p}$$

$$\left(\frac{\partial \bar{\nu}}{\partial E} \right)_{Z_p} = \left(\frac{\partial Z_p}{\partial E} \right)_A / \left(\frac{\partial Z_p}{\partial A} \right)_E$$

Assuming that $\left(\frac{\partial Z_p}{\partial A} \right)_E = \left(\frac{\partial Z_A}{\partial A} \right)_E$, which is equal to 0.38 (Coryell, 1953), $\left(\frac{\partial \bar{\nu}}{\partial E} \right)_{Z_p} = \left(\frac{\partial Z_p}{\partial E} \right)_A / 0.38$. Following this approach, Saha et al found the values of $\frac{\partial \bar{\nu}_h}{\partial E}$ (where $\bar{\nu}_h$ is the average number of neutrons emitted by the heavy fragment) for ^{233}U , ^{235}U , and ^{238}U to be 0.034, 0.072, and 0.066 respectively. They also determined the quantity

$$\frac{\partial \bar{\nu}_T}{\partial E} = \frac{\partial \bar{\nu}_h}{\partial E} + \frac{\partial \bar{\nu}_L}{\partial E}$$
 and then calculated values for $\bar{\nu}_T$, the average total number of neutrons emitted by the fission fragments, by assuming

$$\frac{\partial \bar{\nu}_h}{\partial E} = 2 \frac{\partial \bar{\nu}_c}{\partial E} \quad \text{and} \quad \bar{\nu}_T = \left(\frac{\partial \bar{\nu}_T}{\partial E} \right) E$$
 For the present comparison, the values of Saha et al were substituted into the expression $\bar{\nu}_h = \left(\frac{\partial \bar{\nu}_h}{\partial E} \right) E$. E was taken as the excitation energy of the compound nucleus, since this is the meaning assigned it by Saha et al in their calculations. (The alternative is to determine $\frac{\partial Z_p}{\partial E'}$, and hence $\frac{\partial \bar{\nu}_h}{\partial E'}$ where E' is the excitation energy of the average fissioning nucleus. E' is less than E, but $\frac{\partial Z_p}{\partial E'}$ is correspondingly steeper than $\frac{\partial Z_p}{\partial E}$.) The compound nucleus excitation energies and the resultant values of $\bar{\nu}_h$ are given in Table VI. The heavy fragments resulting from the fission of both ^{235}U and ^{238}U emit twice as many neutrons as the corresponding fragments from the fission of ^{233}U .

In general, the value of N/Z_p for the heavy products is greater for ^{238}U and ^{235}U fission than for ^{233}U at the same energies; that is these products are more neutron rich. The three systems appear to give rise to the same light-mass fragment and product distributions; a comparison was made among heavy products of the three systems having the same charge, and thus descendent from fragments complementary to the same light fragment. The N/Z_p in the case of ^{233}U was used to calculate the most probable charge for a product of mass number 136. This value of Z_p was used to find the mass numbers of the equivalent fission products of ^{235}U and ^{238}U from the values of N/Z_p for those products. The differences in these mass numbers must be the differences in neutron content. The N/Z_p and Z_p values and the mass numbers of these products are given in Table VI.

Tables VII and VIII give the differences in the average number of neutrons involved at each of the three stages discussed above for the pairs of targets $^{233}\text{U} - ^{235}\text{U}$ and $^{233}\text{U} - ^{238}\text{U}$.

Table VII

Comparison of ^{233}U and ^{235}U fission.

proton energy (MeV)	$\Delta\bar{\nu}_{\text{pf}}$	$\Delta\bar{\nu}_{\text{h}}$	$\Delta\bar{\nu}_{\text{remaining}}$	$\Delta\nu_{\text{total}}$
20	0.16	0.96	1.10	2.22
30	0.17	1.34	0.50	2.01
40	0.17	1.72	0.16	2.05
50	0.17	2.09	-0.17	2.09

Table VIII

Comparison of ^{233}U and ^{238}U fission.

proton energy (MeV)	$\Delta\bar{\nu}_{\text{pf}}$	$\Delta\bar{\nu}_{\text{h}}$	$\Delta\nu_{\text{remaining}}$	$\Delta\nu_{\text{total}}$
20	0.53	0.84	3.84	5.21
30	0.61	1.16	3.24	5.01
40	0.64	1.48	2.80	4.93
50	0.65	1.80	2.54	4.99

At each energy, the difference in the average number of pre-fission neutrons, the difference in the average number of neutrons emitted by the heavy fragment, and the difference in the neutron content of the heavy products complementary to the same light product, together equal the difference in the number of neutrons in the two compound nuclei. Thus the data are consistent with the proposition that the nature of the heavy fragment of an asymmetric split is more flexible than that of the light fragment; it is the heavy fragment that absorbs changes in the make-up of the target nucleus, and so a strong target dependence is observed.

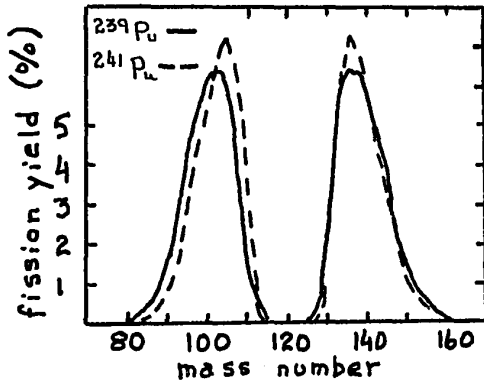


Figure 22.

The mass comparison of the mass distributions from the thermal-neutron fission of ^{239}Pu and ^{241}Pu . The area under the curve is normalized to 200%.

(After Nieler *et al*, 1966)

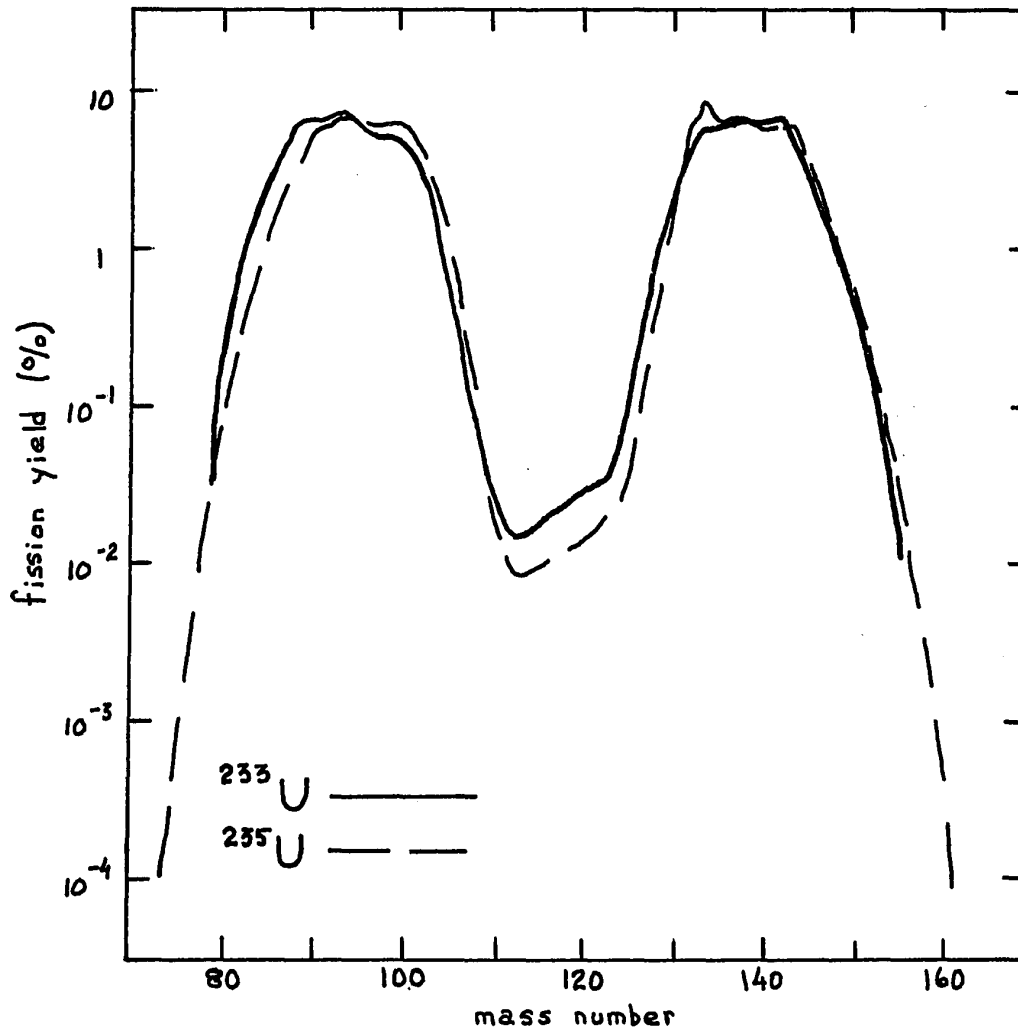


Figure 23. The comparison of the mass distribution from the thermal-neutron fission of ^{233}U and ^{235}U . (After Wahl, 1965)

Nieler *et al* (1966) compared the fragment mass distributions from ^{239}Pu and ^{241}Pu and found that the heavy-fragment mass distributions are almost identical, while the light fragment mass distribution for ^{241}Pu is shifted about two mass units to the right of that for ^{239}Pu , as shown in Figure 22. They suggest that this quantitatively indicates that the two added neutrons in ^{241}Pu appear in the light-mass fragment, and propose that this is due to the higher neutron binding energies in the light fragments relative to their complementary heavy fragments, for $m_H \gtrsim 134$, and to the strong closed-shell effects for $m_H \lesssim 134$. A similar trend is observed in comparing the fragment mass distributions from the thermal-neutron fission of ^{233}U and ^{235}U (Figure 23).

At the excitation energies encountered in the present discussion (25 - 55 MeV) shell effects have little influence on the product distribution (McHugh and Michel). The nucleus is excited well above the fission barrier, and so small neutron binding energy differences between the fragments should not be expected to govern the neutron distribution. A theory consistent with the interpretation proposed in this work must explain not only the differences in neutron distribution but also the differences in the neutron emission characteristics of the heavy fragments. The heavy fragments produced from the fission of ^{235}U and ^{238}U are apparently more excited than those produced from ^{233}U fission, since they emit almost twice as many neutrons. However, the corresponding heavy fragments from ^{235}U and ^{238}U differ from each other by about 2.4 neutrons and yet emit almost equal numbers of neutrons.

References

- Benjamin, P.P., Marsden, D.A., Porile, N.T., and Yaffe, L., *Can. J. Chem.* 47, 301 (1969).
- Bohr, N. and Wheeler, J.A., *Phys. Rev.* 56, 426 (1939).
- Colby, Jr., L.J. and Cobble J.W., *Phys. Rev.* 121, 1410 (1961).
- Coryell, C.D., *Ann. Rev. Nucl. Sci.* 2, 305 (1953).
- Coryell, C.D., Kaplan, M., and Fink, R.D., *Can. J. Chem.* 39, 646 (1961).
- Davies, J.H. and Yaffe, L., *Can. J. Chem.* 41, 762 (1963).
- Flynn, K.F., Glendenin, L.E., and Steinberg, E.P., Argonne National Laboratory, (unpublished). Quoted in The Radiochemistry of Zirconium and Hafnium (ed. E.P. Steinberg), NAS-NS 3011, USAEC (1960).
- Folger, R.L., Stevenson, P.C., and Seaborg, G.T., *Phys. Rev.* 98, 107 (1955).
- Forster, J.H., Porile, N.T., and Yaffe, L., *Can. J. Chem.* 44, 2951 (1966).
- Friedlander, G., Friedman, L., Gordon, B., and Yaffe, L., *Phys. Rev.* 129, 1809 (1963).
- Glendenin, L.E., Coryell, C.D., and Edwards, R.R., Radio-chemical Studies: Fission Products (ed. C.D. Coryell and N. Sugarman), Book I, Paper 52, McGraw-Hill, New York (1951).
- Goeckermann, R.H. and Perlman, I., *Phys. Rev.* 76, 628 (1949).
- Hogan, J.J. and Sugarman, N., *Phys. Rev.* 182, 1210 (1969).
- Huizenga, J.R. and Vandenbosch, R., Nuclear Reactions (ed. P.M. Endt and P.B. Smith), Vol. II. North-Holland, Amsterdam (1962).
- Khan, A.H., Ph.D. Thesis, McGill University, Montreal, Canada (1968).
- Khan, A.H., Saha, G.B., and Yaffe, L., *Can. J. Chem.* 48, 1924 (1970).
- Kraus, K.A. and Moore, G.E., *J. Am. Chem. Soc.* 75, 1460 (1953).
- Lederer, C.M., Hollander, J.M., and Perlman, I., Table of Isotopes (ed. 6). John Wiley and Sons, New York (1967).
- McHugh, J.A. and Michel, M.C., *Phys. Rev.* 172, 1160 (1968).
- Meghir, S., Ph.D. Thesis, McGill University, Montreal, Canada (1962).
- Neiler, J.N., Walter, F.J., and Schmitt, H.W., *Phys. Rev.* 149, 894 (1966).

- Pate, B.D., Foster, J.S., and Yaffe, L., Can. J. Chem. 36, 1691 (1958).
- Present, R.D., Phys. Rev. 72, 7 (1947).
- Saha, G.B., Tomita, I., and Yaffe, L., Can. J. Chem. 49, 2205 (1971).
- Saha, G.B. and Yaffe, L., J. inorg. nucl. Chem. 32, 745 (1970).
- Stevenson, P.C., Hicks, H.G., Nervik, W.E., and Nethaway, D.R., Phys. Rev. 111, 886 (1958).
- Tomita, I. and Yaffe, L., Can. J. Chem. 47, 2921 (1969).
- Wahl, A.C., J. inorg. nucl. Chem. 6, 263 (1958).
- Wahl, A.C., Proc. Symp. Phys. Chem. Fission, Salzburg, Austria, Paper SM-60/22, IAEA (1965).
- Wahl, A.C., Ferguson, R.L., Nethaway, D.R., Trautner, D.E., and Wolfsberg, K., Phys. Rev. 126, 1112 (1962).
- Way, K. and Wigner, E.P., Radiochemical Studies: Fission Products (ed. C.D. Coryell and N. Sugarman), Book I, Paper 43. McGraw-Hill, New York (1951).
- Wiles, D. and Coryell, C.D., Phys. Rev. 96, 696 (1954). Quoted in The Radiochemistry of Molybdenum (ed. E.M. Scadden and N.E. Ballou), NAS-NS 3009, USAEC (1960).
- Yaffe, L., Proc. Symp. Phys. Chem. Fission, Vienna, Austria, Paper SM-122/3, IAEA (1969).